공학박사 학위논문

Development of Mixed Metal Oxide Catalysts for Oxidative Dehydrogenation of Ethane to Ethylene

에탄 산화탈수소화반응을 통해 에틸렌을 생산하기 위한 혼합금속산화물 촉매 개발

2017년 8월

서울대학교 대학원

화학생물공학부

이 민 재

Abstract

Development of Mixed Metal Oxide Catalysts for Oxidative Dehydrogenation of Ethane to Ethylene

Minzae Lee

School of Chemical and Biological Engineering

The Graduate School

Seoul National University

The increasing demand for light olefins and the changing nature of upstream feedstock boosted up the substantial research activity into the development of alternative process routes. Ethylene is one of the most widely required primary building blocks for the preparation of value-added chemical products (*e.g.*, polyethylene, ethylene oxide, ethylene glycol, styrene, vinyl acetate monomers, and polyvinyl chloride etc.) and many other intermediate products in current society.

A steam cracking method, under high temperature pyrolysis in the presence of diluting steam, is the most settled industrial process for the manufacture of ethylene. Feedstocks for the steam cracking method have mostly been naphtha and natural gases in this process. Currently the basic feedstock for steam cracking has only shifted to ethane in the last decade, thus leading to attractive production costs. It should be noted that the emerging availability of shale gas will remarkably shift the overall petrochemical industry towards processes that use light alkanes to production of ethylene.

The increase in the price of crude oil, in particular, and the availability of ethane from shale gas, has led to the interest in alternative processes for ethylene production, such as oxidative dehydrogenation of ethane (ODHE).

This process offers diverse advantages, thus it has been attracting considerable attentions as a subject of substantial research activities. However, the lack of suitable catalysts that combine high activity and selectivity has prevented their industrial realization so far.

In an attempt to develop efficient catalyst for the reaction, both the exterior and interior design of active catalysts was performed as below:

- Ni-Nb-O mixed oxide embedded on $Ce_xZr_{1-x}O_2$ (denoted herein as Ni-Nb-O/$Ce_xZr_{1-x}O_2$), which is a concept of exterior design, were designed based on the insights into reaction pathways. Compared with using Ni-Nb-O alone, the introduction of $Ce_xZr_{1-x}O_2$ to the Ni-Nb-O active catalyst contributes on suppressing the formation of byproducts (CO, CO_2, and CH_4) at relatively high reaction temperature (450 °C). The increased reaction temperature also leads to an enhancement of ethane conversion (~55%) and subsequent increase in the production of ethylene (6.3 $\mu mol_{gactive\ cat}^{-1}\ s^{-1}$), compared to that of conventional Ni-Nb-O catalyst (1.5 $\mu mol_{gactive\ cat}^{-1}\ s^{-1}$). Relevant control tests and the electrochemical tests suggest that the promotion effect of $Ce_xZr_{1-x}O_2$ additive is attributed to the compensation of lattice oxygen from $Ce_xZr_{1-x}O_2$ into the lattice oxygen vacancy in Ni-Nb-O active catalysts, which originates from consumed lattice oxygen during the ethane conversion.
- Ce-incorporated MoVTeNbO, which is a concept of interior design, was designed to improve catalytic activity with exhibiting almost 100% ethylene selectivity from ODHE process. In this study, the effect of Ce in MoVTeNbO was intensively characterized. Activation temperature (600 °C) and amount of Ce atom (0.1 atom%) are optimized as attempts to maximize the ratio of reactive phase, M1 phase (unique structure for Mo-V based mixed metal oxide), for the selective production of ethylene. As a result, the Ce-incorporated MoVTeNbO catalyst exhibited

comparable ethylene yield (~60 %) with reducing reaction temperature (~50 °C) during the ODHE process, compared to pure MoVTeNbO catalyst. Results of physicochemical characterizations suggest that the improved catalytic performance of Ce-incorporated MoVTeNbO should corresponds with the location of Ce atoms in the lattice structure of M1 phase MoVTeNbO, and subsequent improvements in redox property of active sites.

Keywords: heterogeneous catalyst, oxidative dehydrogenation, ethane, ethylene, lattice oxygen

Student Number: 2013-31305

Contents

List of Tables

List of Figures

Chapter 1. Introduction

1.1 Current practice: Steam cracking and oxidative dehydrogenation of ethane

1.1.1 Steam cracking

The steam cracking of hydrocarbons (*e.g.*, naphtha, natural gas, and ethane) is the most widely used process for the industrial production of ethylene. The alkanes and steam as feedstocks are converted into ethylene and other residuals at relatively high temperature (800~1200 °C) in tubular reactors. In more details, feedstocks with boiling point up to 600 °C can be converted and/or cracked through a radical chain pathway. Over the past 50 years, this process has been developed and optimized a lot. The feed is converted into small olefins and di-olefins through this pyrolysis process. Since the high reactivity of the olefin products, the effluent has to be cooled down within 0.02-0.1 seconds to avoid further conversion of olefins. And then, the products are separated by a distillation and absorption/adsorption processes together.

Main parameters that determine the conversion performance and distribution of products are known to be residence time, reaction temperature, and inlet pressure in the reactor. The level of primary conversion is around 70 %, with olefin yields of ~50 % using ethane as a feed, whereas conversion

and yields for the naphtha crackers are lower than those of ethane cracker.

Since the cracking process occurs at very high temperatures with high amounts of reactant streams, strict use of equipments is required. Piping systems and reactors should be composed of heat-resistant material and settlement of several heat exchangers is essential.

Although these processes are regarded as an industry standard for ethylene production, steam cracking method accompanies several limitations. Consumed level of energy is very high of ~16 GJ t^{-1} for ethane cracking and ~23 GJ t^{-1} for naphtha cracking because the cracking process is endothermic reaction [1]. During the process, a part of the light effluent from the product is recycled to the main feed again for continuous combustion inside the reactor, leading to the formation of CO_x and NO_x. Furthermore, this combustion process results in the formation of severe cokes on the inside the reactor walls, leading to a requirement of periodic and/or frequent maintenance to remove them.

1.1.2 Oxidative dehydrogenation of ethane (ODHE)

As an alternative method for the production of ethylene to the above steam cracking method, oxidative dehydrogenation of ethane (ODHE) has currently attracted great attention [2-8]. ODHE processes can exhibit high ethane conversion than that of direct dehydrogenation of ethane at lower reaction temperature (about 350 ~ 600 °C), and compared to steam cracking. Moreover, reaction is exothermic, which leads to growing interest in this

process (Eq. (1)) [9-12].

$$C_2H_6 + 0.5O_2 \rightarrow C_2H_4 + H_2O \ (\Delta H = -105.5 \text{ kJ mol}^{-1}) \quad (1)$$

Ethane has normally been extracted from natural gas and shale gas, which is abundant and getting cheaper as the development of shale-gas industry continues. In this sense, ethane can be a suitable feedstock for oxidative dehydrogenation for the production of ethylene. In the ODHE process, O_2 is inserted into feed with ethane and catalystic reaction occurs during the reaction. The development of suitable catalysts is one of the challenging points for further scale-up, because olefins are more reactive than the reacting alkanes. This higher reactivity of the olefins is attributed to the characteristics toward direct bonding on the surface of catalyst, whereas alkanes interact via dispersion force.

Since ethylene is produced by ethane through dehydrogenation procedure using O_2, formation of byproducts (CO_x) and water can take place via total oxidation of ethane and/or over-oxidation of ethylene. This reaction pathway is mostly attributed to the oxygen reacts with the C-H bond during the primary activation or addition of oxygen into ethylene as shown in Fig. 1 [13].

In short, suppression of such byproducts to reach high ethylene selectivity with high ethane conversion at low temperature is the desired performance what ODHE process should targeted. In order to achieve this goal of ODHE process, the catalysts should favor hydrogen abstraction, as well as

minimization of oxygen insertion into ethane molecules. The emerging paradigm in the development of efficient catalysts is that design of the physicochemical properties of them through fundamental insight into the reaction mechanism on a molecular level, including the details of the interactions with catalytic surfaces and the associated gas-phase reactions [14].

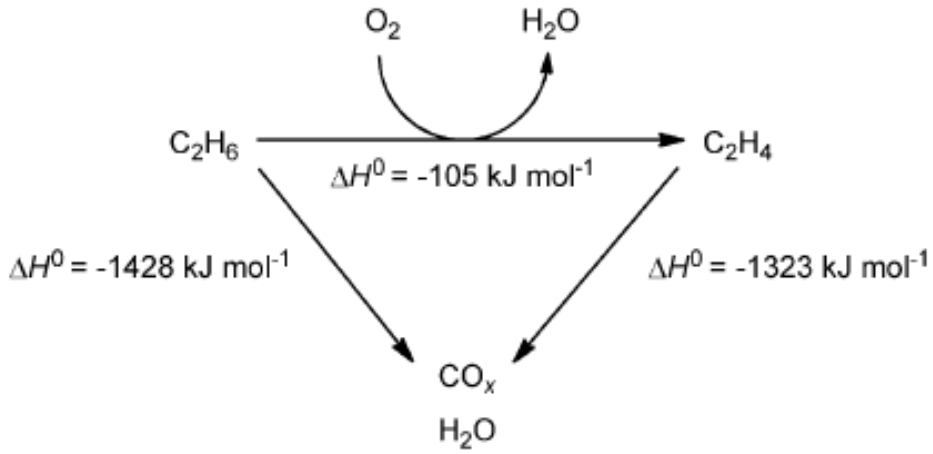

Fig. 1-1. ODH reaction of ethane with side reactions.

1.2 Single and paired-electron process for ODHE

In all, the C-H cleavage procedure is governed by two processes, which are homolytical (single electron) and heterolytical (paired electron) processes, respectively. The energy barrier to overcome for the activation of ethane for homolytical process is higher than that of the heterolytical process. In the case of homolytical process, the reaction should involve thermal and/or radical-induced reactions as shown in Fig. 2 [15].

Since the presence of difficulties in the control of free-radical based gas-phase reactions, surface catalytic processes are much more promising for further facilitation. It is widely accepted that most of the reaction mechanism for surface catalytic reactions are followed by the simultaneous transfer of two electrons. Rate determining step (RDS) of the mechanism is the cleavage of C-H bond in ethane heterolytically. In general, proton abstraction firstly occurs on strong basic sites on the surface of catalyst, leading to heterolytic cleavage of a C-H bond. It is still on a controversy that such sites are provided from nucleophilic lattice oxygen or electrophilic metal cation in metal oxide catalyst [16,17]. Typical catalytic redox reaction cycle that shows transfer of an electron pair in Molybdenum oxide as an example is illustrated in Fig. 3 [18].

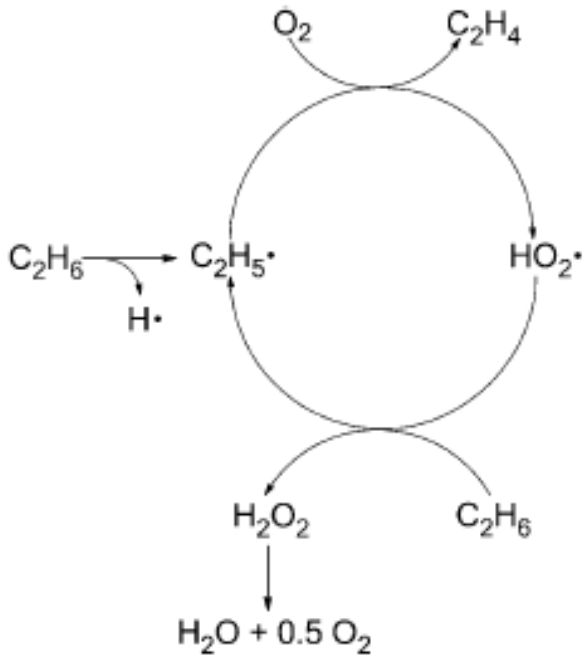

Fig. 1-2. Single-electron process for C-H bond activation.

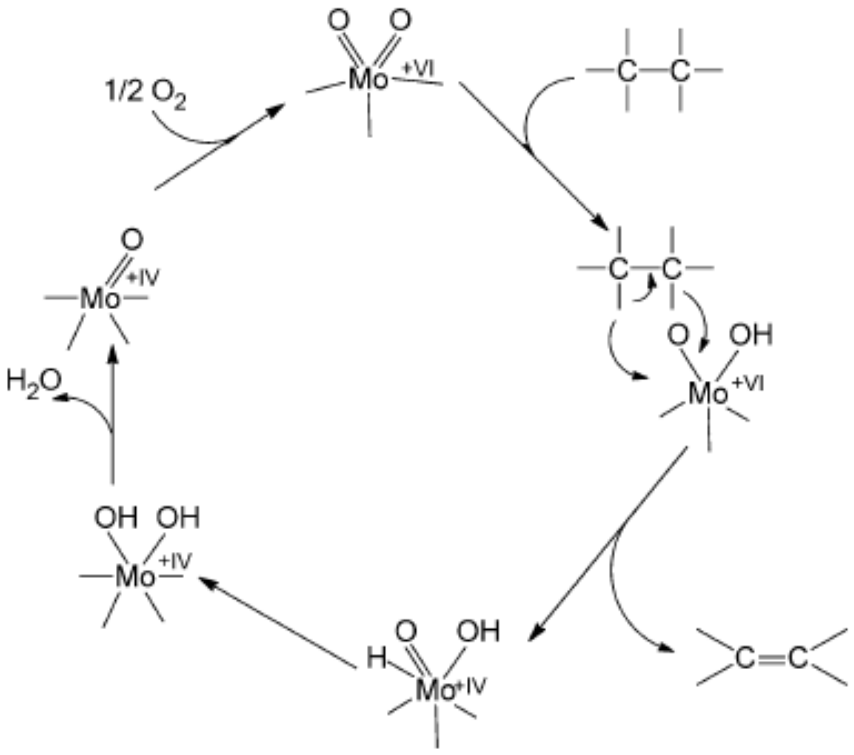

Fig. 1-3. Redox cycle over Mo, which involves a paired electron transfer.

1.3 Active sites for the ODHE of ethane

Qualification and quantification of active sites of catalyst for use in ODHE process have much more been highlighted during the design of catalyst due to their importance on determining catalytic activity and product selectivity. Several metal oxide catalysts that contain anions and redox-active metal cations during the redox cycle have been developed [19-26]. ODHE reaction has been reported that it follows Mars-van Krevelen mechanism on such metal oxide catalyst [27]. At first, an ethoxy-hydroxy pair is formed from ethane, which reacts with the surface of metal oxide catalyst (Fig. 3.). In this step, C-H bond is cleaved and subsequent formation and desorption of ethylene take place, leaving dihydroxy species on the catalyst surface. The dihydroxy species acts as a removal of water molecule that is formed during the first step, leading to the reduction of metal oxide sequentially [28]. After that, the reduced surface of metal oxide is re-oxidized by reacting with the fed O_2.

1.4 Parameters for determining activity and selectivity

1.4.1 Metal-oxygen bond strength

One of the most important factors that directly influences on the catalytic activity and product selectivity is the metal-oxygen (M-O) bond in the active site of catalyst. More specifically, the bond strength and its variation with the degree of reductive behavior are important for redox-active metal oxide catalyst [29]. The catalytic activity and the product selectivity go through a maximum point in terms of the formation rate of the partial oxidation product (*i.e.*, ethylene) as this bond strength varies, and thus the volcano plots can be obtained as a function of ethylene yield.

If the M-O bond strength is strong, the lattice oxygen on the surface of catalyst would not react with the ethane molecule, which results in the decrease of ethane conversion level. In this case, suppression of multiple oxidations is suppressed, and thereby the ethylene selectivity will increase [30]. If the M-O bond strength is weak, reverse results (*i.e.*, high ethane conversion level and low ethylene selecitivy) can be obtained due to the presence of multiple oxidation steps [31].

The M-O bond strength is related to the oxidation state of the metal cations in metal oxdies. The M-O bond strength generally increases as the increase of the oxidation state of metal cations. If the one metal cation site is bonded with more than one lattice oxygen atom, the release of the second oxygen atom after the initial reduction step is much more difficult than the

first, for example, in a metal site combined with a non-reducible oxide site [32].

1.4.2 Role of O^- and O^{2-}

Intensitve studies have been done to clarify the effects of O^- and/or O^{2-} on the product selectivity for ODHE process [33]. Results of DFT calculations and thermodynamical studies have demonstrated that the byproduct is readily formed, mainly CO_x, from ethane when O^- reacts with ethane molecule. And this O^- is generated by surface hole of metal oxide catalyst. In contrast to the role of O^-, the O^{2-} plays an important role for production of ethylene. And it is generally accepted that this O^{2-} is provided by the lattice oxygen of metal oxide catalyst. Therefore, it is shortly summarized that minimization of amount of holes and enhancement of redox property for metal oxide catalyst are potential strategies to develop an efficient catalysts for ODHE process to ethylene.

1.4.3 Desorption and re-adsorption of ethane

Ethylene tends to adsorb on the surface of catalysts rather than ethane due to higher reactivity of ethylene, compared to ethane. When ethylene is re-adsorb on the catalyst surface, it is possible that the ethylene is oxidized again (over-oxidation of ethylene), which leads to lowering of the ethylene selectivity. Optimizing specific surface area of the catalyst can be the first

option to overcome the re-adsorption of ethylene and subsequent over-oxidation. The second concept to unravel this limitation is site isolation, which increases the selectivity for partial-oxidation products. Becase active sites with more than two labile lattice oxygen atoms facilitate oxygen insertion before desorption, thus eventually leading to CO_x species [34-38].

1.5 Objective

This thesis mainly consists of the development of mixed metal oxide catalytic materials to improve redox property of mixed metal oxide catalyst via (1) external and (2) internal promotion strategies toward ODHE reactions.

(1) In Chapter 2, improved redox property for Ni-Nb-O active catalyst embedded on $Ce_xZr_{1-x}O_2$ (=Ni-Nb-O/$Ce_xZr_{1-x}O_2$) and its effects toward ODHE reaction to ethylene is discussed. Introduction of $Ce_xZr_{1-x}O_2$ into Ni-Nb-O confers significantly improved redox property and reduced nonstoichiometric Ni^{2+} sites, compared to Ni-Nb-O only. Chemically interacted Ni-Nb-O/$Ce_xZr_{1-x}O_2$ greatly improved the catalytic performance for both ethane conversion and ethylene selectivity, compared to physically mixed Ni-Nb-O+ $Ce_xZr_{1-x}O_2$ catalyst. This promotion should be compensation of oxygen vacancy in Ni-Nb-O from $Ce_xZr_{1-x}O_2$ via hopping of lattice oxygen.

(2) In Chapter 3, Ce-doped MoVTeNbO mixed metal oxide catalysts are presented. Incorporation of excellent redox property of Cerium atoms within the lattice structure of MoVTeNbO dramatically increases the physicochemical properties of active sites. Optimum amount of Ce contents were investigated to maintain active phase to production of ethylene via ODHE process. The level of ethane conversion greatly improved, which results in the saving consumed energy via reduction of reaction temperature (~50 °C), with exhibiting comparable catalytic performance to MoVTeNbO only.

Chapter 2. Enhanced ethylene productivity by promotion of lattice oxygen in Ni-Nb-O/$Ce_xZr_{1-x}O_2$ composite for oxidative dehydrogenation of ethane

2.1 Introduction

Metal-doped NiO (Ni-Me-O) is one of the promising catalysts for ODHE reaction at low reaction temperature to around ≤420 °C [39-43]. The low reaction temperature, however, limits level of ethane conversion to 30-35%, which prohibits further improvement of ethylene productivity [41]. The presence of this limitation would be due to the difficulties in maintaining high ethylene selectivity at high reaction temperature. Although increase in reaction temperature may boost the level of ethane conversion, ethanemolecules mostly tend to be converted into various byproducts (*e.g.*, CO, CO_2 and CH_4) at high reaction temperature, which can extremely deteriorate the ethylene selectivity.

Strategies for proper solving these issues should target their fundamental origins. The reaction pathway for the ODHE reaction on Ni-Me-O is governed by the Mars-van Krevelen mechanism, which consumes lattice oxygen within the catalyst to produce ethylene [44,45]. It has clearly been stated that the byproducts can be produced by the surface oxygen generated

by surface positive holes (h^+) from metal doped Ni mixed oxide [42]. Therefore, aforementioned limitations could be explained by this theoretical approach, which might be ascribed to the insufficient reactive lattice oxygen capability within the Ni-Me-O at high reaction temperature. On the basis of this reaction mechanism, enabling of a rapid uptake and release of lattice oxygen can be an effective strategy to improve the catalytic properties of Ni-Me-O and increases ethylene production via the ODHE process.

$Ce_xZr_{1-x}O_2$ mixed oxide has been studied as a materialwith excellent oxygen storage and release capacity (OSC) due to its unique redox properties [46-48]. Thus, the introduction of such a mixed oxide into the Ni-Me-O could improve the uptake and release characteristics of lattice oxygen within the Ni-Me-O catalyst. It is believed that supplying of lattice oxygen from $Ce_xZr_{1-x}O_2$ to Ni-Me-O can be achieved via chemical interaction between these two materials, because lattice oxygen transfer occurs by hopping and/or diffusion through its vacancy sites [49]. With the introduction of this strategy, it is expected that reaction temperature limitations diminish as a better supply of lattice oxygen reduces the number of holes and leads to the formation of ethylene rather than byproducts at temperatures exceeding 420 °C, which also allows increase in level of ethane conversion.

In this study, we report on a development of Ni-Me-O/$Ce_xZr_{1-x}O_2$ composites as an efficient catalyst for the production of ethylene via ODHE reaction. Niobium (Nb) was selected as a replacement for Me in Ni-Me-O, which serves as a ‘model’ active catalyst based on its high catalytic performance in the ODHE reaction [42,45,50]. Main objective focuses on the

improvement of ethylene productivity via increase in reaction temperature with suppressing formation of byproducts using Ni-Me-O/$Ce_xZr_{1-x}O_2$ catalyst.

2.2 Experimental

2.2.1 Preparation of catalysts

A series of N-Nb-O/$Ce_xZr_{1-x}O_2$ catalysts were prepared by varying the molar ratio of cerium and zirconium at 3:7, 5:5, and 7:3, and the total loading amount of Ni-Nb-O was 20 wt% in the Ni-Nb-O/$Ce_xZr_{1-x}O_2$. At first, $Ce_xZr_{1-x}O_2$ series were prepared using a co-precipitation method with aqueous solutions of zirconium(IV) oxynitrate hydrate (Aldrich, $ZrO(NO_3)_2 \cdot 2H_2O$, 99.0%) and cerium(III) nitrate hexahydrate (Aldrich, $Ce(NO_3)_3 \cdot 6H_2O$, 99.0%) [51]. The pH was controlled at ~ 9 using an aqueous solution of ammonia (0.6 M) under vigorous stirring. After 4 h of aging, the dispersion was filtered with deionized water and dried at 60 °C for 12 h, then finally calcined under air at 650 °C for 5 h. The Ni-Nb-O mixed oxides were then loaded onto as-prepared $Ce_xZr_{1-x}O_2$ using an impregnation/evaporation method. $Ce_xZr_{1-x}O_2$ powder was mixed with the aqueous solutions of nickel(II) nitrate hexahydrate (Sigma-Aldrich, $N_2NiO_6 \cdot 6H_2O$, 99.999%) and ammonium niobate(V) oxalate hydrate (Aldrich, $NC_4H_4NbO_9 \cdot xH_2O$, 99.99%) and heated at 80 °C to accelerate the evaporation of the solvent [52]. The resultant slurry was dried in a vacuum oven at 60 °C for 12 h and calcined under air at 450 °C for 5 h. The atomic Nb/Ni ratio was controlled at 0.176 as a model composition based on previous reports [53]. In the present study, Ni-Nb-O/$Ce_{0.3}Zr_{0.7}O_2$, Ni-Nb-O/$Ce_{0.5}Zr_{0.5}O_2$, and Ni-Nb-O/$Ce_{0.3}Zr_{0.5}O_2$ are denoted as Ni-Nb-O/CZ37, Ni-Nb-O/CZ55, and Ni-Nb-

O/CZ73, respectively.

Ni-Nb-O/CeO_2 and Ni-Nb-O/ZrO_2 were also prepared to compare catalytic performance of Ni-Nb-O/CZ series. The synthetic procedures for Ni-Nb-O/CeO_2 and Ni-Nb-O/ZrO_2 were identical to those of the Ni-Nb-O/CZ series. The total loading amount of Ni-Nb-O was 20 wt% for both Ni-Nb-O/CeO_2 and Ni-Nb-O/ZrO_2.

To verify the effect of chemical interaction between Ni-Nb-O active catalyst and a CZ37 (=$Ce_{0.3}Zr_{0.7}O_2$) for Ni-Nb-O/CZ37 catalyst to the catalytic performance, we prepared "Ni-Nb-O+CZ37_phys" by physically mixing bulk Ni-Nb-O and CZ37. The powders of bulk Ni-Nb-O and $Ce_{0.3}Zr_{0.7}O_2$ were grinded together for 30 min. In prior to their mixing, the amounts of Ni-Nb-O and CZ37 for the "Ni-Nb-O+CZ37_phys" were controlled to match an as-prepared Ni-Nb-O/CZ37.

Bulk Ni-Nb-O was synthesized using the aforementioned evaporation method to allow further comparisons of catalytic performance with Ni-Nb-O/$Ce_xZr_{1-x}O_2$ and as a source for the preparation of Ni-Nb-O/CZ37_phys. In the synthesis of bulk Ni-Nb-O, the only difference was the absence of $Ce_xZr_{1-x}O_2$ powder.

2.2.2 Characterizations

An X-ray diffractometer (XRD, Rigaku, D/max-2500/PC) using Cu Kα radiation (wavelength = 0.154 nm) as an incident beam at 50 kV and 100 mA was utilized to confirm the crystalline size and elemental phases of the

prepared composites. N_2 adsorption-desorption isotherms were measured with a Micromeritics ASAP 2010 instrument. The Brunauer-Emmett-Teller (BET) method was utilized to calculate the specific surface area. X-ray photoelectron spectroscopy (XPS, Kratos, AXIS-HSI) was used to investigate the elemental species and the binding states of the prepared samples. Atomic-distribution mapping was performed using high angle annular dark field (HAADF)-scanning transmission electron microscopy (STEM) (JEM-2100F, 200 kV) to observe the features of existing atomic species (Ni, Nb, O, Ce, and Zr). To examine the reducibility of the prepared catalysts, temperature programmed reduction (TPR, AutoChem II, Micromeritics) was conducted using a thermal conductivity detector (TCD) with 10% hydrogen in argon and 0.03 g of catalyst in a conventional TPR set-up. The temperature was linearly ramped up to 1073 K at a rate of 10 K min^{-1}.

2.2.3 Electrochemical tests

All electrochemical experiments were performed with an Iviumstat workstation in a three-electrode cell. Rotating disk electrode (RDE) was used for the measurement. A catalyst loaded glassy carbon electrode (GCE, 5 mm dia.), an Ag/AgCl electrode (KCl saturated) and a platinum electrode served as working, reference and counter electrodes, respectively.

Catalyst inks were prepared by the following order. As-prepared catalysts (10 mg) were mixed with 20 μL deionized water for stable mixing with the

binder in the next step. 57 μL of 5% Nafion and 800 μL of isopropyl alcohol were then inserted under vigorous stirring and sonication for both the 30 min. 7.0 μL of each ink was dropped onto the GCE and dried at room temperature. The cyclic voltammetry (CV) tests were performed between -0.1 and 0.7 V (vs. Ag/AgCl) with a scan rate of 10 mV s^{-1} in O_2 saturated 0.1 M KOH aqueous solution.

2.2.4 Catalytic reaction tests

The oxidative dehydrogenation (ODH) of ethane was performed in a fixed bed reactor (a quartz tube with 8 mm i.d. and a length of 290 mm). The reaction temperature was varied from 350 to 500 °C under atmospheric pressure. A thermocouple was installed at the outer surface of the reactor near the catalyst bed in order to measure the reaction temperature. The gas feed consisted of $C_2H_6/O_2/He/N_2$ with a 10/5/60/25 molar ratio at a total flow rate of 20 cm^3 min^{-1}. The used amount of catalyst was 0.3 g. He and N_2 gases were used as an inert gas and an internal standard gas, respectively.

The reactants and products were analyzed using an on-line gas chromatograph (GC, ACME 6100, Younglin Instrument) equipped with both a flame ionization detector (FID) and a thermal conductivity detector (TCD). The FID was used for a more precise detection of hydrocarbons. Two columns were used in the analysis, a Porapak Q (CO_2, C_2H_4, C_2H_6) and a Molsieve 13X (N_2, O_2, CO). The ethane conversion and ethylene selectivity were defined on a carbon basis. The acquired experimental data were

calculated using the following equations:

$$X_{C_2H_6} = \frac{f_{C_2H_6\,(in)} - f_{C_2H_6\,(out)}}{f_{C_2H_6\,(in)}} \times 100\ (\%) \quad (1)$$

$$S_{C_2H_4} = \frac{f_{C_2H_4\,(out)}}{f_{C_2H_6\,(in)} - f_{C_2H_6\,(out)}} \times 100\ (\%) \quad (2)$$

where $X_{C_2H_6}$ is the ethane conversion, $S_{C_2H_4}$ is the selectivity to ethylene, and f is the molar flow rate in the effluent gas. For each test, the detected chemical mixture with C_2H_6, C_2H_4, and CO_2 gives an almost close carbon balance of 100%. CH_4 and CO were not detected under our measurement conditions.

2.3 Results and discussion

2.3.1 Catalyst characterizations

Structural characterization was performed via XRD analyses to observe the phase of the Ni-Nb-O/CZs and to measure the crystalline sizes of Ni-Nb-O in them (Fig. 2-1 and Table 2-1). The results show that a structural phase of the $Ce_xZr_{1-x}O_2$ solid solution for Ni-Nb-O/CZ37, Ni-Nb-O/CZ55, and Ni-Nb-O/CZ73 is dependent on Ce/Zr molar ratio based on the fact that cubic and tetragonal phases were observed for Ni-Nb-O/CZ73 and Ni-Nb-O/CZ37, respectively. This shift is attributed to the incorporation of smaller Zr^{4+} (ionic radii of 0.84 Å) into the CeO_2 (ionic radii of 0.97 Å) lattice [54,55]. Moreover, it was confirmed that Ni-Nb-O has the pure NiO crystallizes in the cubic rock salt structure. In addition, Ni-Nb-O mixed oxides for prepared samples are composed of crystallites in the nanorange (13-20 nm), which were confirmed by Scherrer equation. The presence of Nb disturbs crystallization of NiO, and therefore small grain sizes are obtained [56]. The absence of a pure Nb_2O_5 peak for Ni-Nb-O indicates that the Nb atoms are well incorporated into the lattice NiO catalyst [57]. Despite introduction of the Ni-Nb-O to $Ce_xZr_{1-x}O_2$ in constructing the composites, the structural phases of both were well maintained in Ni-Nb-O/CZ37, Ni-Nb-O/CZ55, and Ni-Nb-O/CZ73 without forming additional phases (*e.g.*, Ni-Ce, Ni-Zr, Nb-Ce, and Nb-Zr composites), as shown in Fig. 2-2 and Fig. 2-3. The crystalline sizes of Ni-Nb-O for Ni-Nb-O/CZs were smaller than that for

bulk Ni-Nb-O, which indicates the presence of $Ce_xZr_{1-x}O_2$ participated in the determination of crystalline size of Ni-Nb-O during the formation of Ni-Nb-O.

The composition and the specific surface areas of the Ni-Nb-O/CZ series (=Ni-Nb-O/CZs) are present in Table 2-1. The specific surface areas of the Ni-Nb-O/CZs were measured and compared with that of bulk Ni-Nb-O (without CZs) by N_2 sorption isotherms. The specific surface area of Ni-Nb-O/CZ37 was lower than those for Ni-Nb-O/CZ55 and Ni-Nb-O/CZ73, whereas the surface area for bulk Ni-Nb-O was 3.4 times higher than that for Ni-Nb-O/CZ37. The proportional changes in specific surface area to the cerium content for the Ni-Nb-O/CZs can be ascribed to an enlargement of the lattice parameter within $Ce_xZr_{1-x}O_2$ (Table 2-2), which is in good agreement with a previous report [47]. Note that the specific surface areas of the Ni-Nb-O/CZs are much lower than that of the bulk Ni-Nb-O, which reflects that Ni-Nb-O particles in Ni-Nb-O/CZs catalysts can be present as a polycrystalline structure and/or their size of particles are bigger than that of the bulk Ni-Nb-O.

In order to examine the reducibility of the Ni-Nb-O/CZ37, Ni-Nb-O/CZ55, and Ni-Nb-O/CZ73 composites, H_2-TPR analyses were performed (Fig. 2-4). The H_2-TPR spectra show that the reduction temperatures at maximum H_2 uptake for Ni-Nb-O/CZ37, Ni-Nb-O/CZ55, and Ni-Nb-O/CZ73 were 347, 368, and 371 ˚C, respectively. The lowest reduction temperature for Ni-Nb-O/CZ37 implies that this sample has the highest reactivity of lattice oxygen toward β-hydrogen elimination, and that the subsequent formation of

ethylene would be easier than it would be for Ni-Nb-O/CZ55 and Ni-Nb-O/CZ73 [41]. The peaks recorded at the lowest temperature for all samples are originated from the oxygen species located on the surface of Ni-Nb-O and/or $Ce_xZr_{1-x}O_2$ [41,58]. We also confirmed that the Ni-Nb-O particles are highly distributed with $Ce_{0.3}Zr_{0.7}O_2$ (=CZ37) for Ni-Nb-O/CZ37, which is important to maximize the promotion effects for an enhanced production of ethylene in the ODHE reaction (Fig. 2-5). The XPS results indicate that the prepared Ni-Nb-O for Ni-Nb-O/CZs consists of the NiO structure, which are in good agreement with the observation from XRD analyses (Fig. 2-6). It should be noted that main oxidation states of the Ni is Ni^{2+} for Ni-Nb-O/CZs, which reveals that the Ni-Nb-O mixed oxides for Ni-Nb-O/CZs can suppress the formation of non-stoichiometric structure in NiO [41]. The low concentration of low non-stoichiometric oxygen in the Ni-Nb-O implies that the catalytic production of ethylene can be improved in the ODHE reaction.

2.3.2 Catalytic performance in the ODH of ethane

Values for ethane conversion and ethylene selectivity obtained in the catalytic ODH reaction at temperatures ranging from 350-500 ˚C for the bulk Ni-Nb-O and Ni-Nb-O/CZ series are presented in Fig. 2-7 and Fig. 2-8, respectively. A higher level of ethane conversion (~55%) for Ni-Nb-O/CZ37 at 450 ˚C was achieved compared with that for bulk Ni-Nb-O (~38%) at 400 ˚C via the rising in reaction temperature during the production of ethylene. Moreover, ethylene was more selectively produced for Ni-Nb-O/CZ37 than

that for bulk Ni-Nb-O at tested reaction temperatures. These enhanced catalytic performances of Ni-Nb-O with combining CZ37 can lead to the improved ethylene production. All of ethane molecules were converted into other chemical species at 450 and 500 ˚C for bulk Ni-Nb-O and Ni-Nb-O/CZs, respectively. The 100% conversion of ethane is associated with the formation of byproducts (CO_2, CO, and CH_4), meaning that the production of ethylene was fully hampered (Table 2-3). CO_2 was the only byproduct observed under our testing condition during the production of ethylene (≤ 450 ºC for Ni-Nb-O/CZs and ≤ 400 ºC for Ni-Nb-O). The superior ethylene selectivity for Ni-Nb-O/CZ37 than that for bulk Ni-Nb-O at tested range of reaction temperature might be ascribed to the presence of larger amount of reactive lattice oxygen within the Ni-Nb-O/CZ37 than that for other bulk Ni-Nb-O. It should be noted that the production of ethylene is related to the lattice oxygen only. Ethane conversion increased as a function of reaction temperature for all as-prepared Ni-Nb-O/CZs and ethylene selectivity for Ni-Nb-O/CZ37 was higher than those for Ni-Nb-O/CZ55 and Ni-Nb-O/CZ73 in the temperature range studied. A consistent decreasing trend (5~10%) of ethylene selectivity for Ni-Nb-O/CZ37 as a function of reaction temperature (ΔT=50 ºC) indicates that CO_2 is mostly formed by complete ethane oxidation rather than by ethylene over-oxidation [59].

For successful delivery of the lattice oxygen from the $Ce_xZr_{1-x}O_2$ to the Ni-Nb-O active catalyst, there should be intimate chemical interaction between them. In order to verify the presence of chemical interaction between Ni-Nb-O and $Ce_xZr_{1-x}O_2$ in Ni-Nb-O/CZ37, and to evaluate the effects of chemical

interaction to catalytic performance, we compared Ni-Nb-O/CZ37 with Ni-Nb-O+CZ37_phys (see experimental section). Ethane conversion and ethylene selectivity obtained in the reaction temperature range of 350-450 ˚C for Ni-Nb-O/CZ37 and Ni-Nb-O+CZ_phys are presented in Fig. 2-9 and Fig. 2-10, respectively. The value and the trend of increasing ethane conversion for physically mixed sample were similar to those of Ni-Nb-O/CZ37 at 350 ˚C and 400 ˚C. The ethylene selectivity for the Ni-Nb-O/CZ37 was slightly higher than that of the physically mixed version at temperature range studied. All of the ethane molecules were converted into byproducts (CO_2, CO, and CH_4) at 450 ˚C for physically mixed sample. This can be interpreted as better supply of lattice oxygen was achieved through the chemical interaction between $Ce_xZr_{1-x}O_2$ and the Ni-Nb-O in Ni-Nb-O/CZ37 than that of the physically mixed version. Moreover, the important role of such a chemical interaction is highlighted by the prohibited production of ethylene for the physically mixed sample at 450 ˚C.

The CeO_2, ZrO_2, and $Ce_xZr_{1-x}O_2$ (x=0.3, 0.5, and 0.7, respectively) all recorded negligibly low levels of ethylene productivity at 450 ˚C (Table 2-4). Thus, it is reasonable to compare catalytic performances among only the Ni-Nb-O mixed oxides as an active catalyst. To examine the changes in catalytic behavior before and after the introduction of $Ce_xZr_{1-x}O_2$ on the Ni-Nb-O active catalyst toward the ODHE process, we compared the ethylene productivity per mass of Ni-Nb-O at 450 ˚C for the prepared samples (Fig. 2-11). The corresponding result for bulk Ni-Nb-O performed at 400 ˚C was also compared because bulk Ni-Nb-O showed the maximum ethylene

productivity at this reaction temperature. Ni-Nb-O/CZ37 showed the highest ethylene productivity at 450 ˚C, and followed by Ni-Nb-O/CZ55 and Ni-Nb-O/CZ73. Ni-Nb-O/CeO_2 and Ni-Nb-O/ZrO_2 exhibited inferior ethylene productivity to those of Ni-Nb-O/CZs. The highest ethylene productivity for Ni-Nb-O/CZ37 among these samples is due to the highest ethylene selectivity (~50.2%) and the highest ethane conversion (~55%) at 450 ˚C. Incorporation of small metal heteroatoms (*e.g.*, zirconium) into cerium oxide leads to an increase in the space surrounding lattice oxygen, facilitating reversible storage and release of oxygen into the lattice matrix [60]. Therefore, the high ethylene selectivity for Ni-Nb-O/CZ37 can be due to its excellent OSC, comparing with those of Ni-Nb-O/CeO_2, Ni-Nb-O/ZrO_2, and other Ni-Nb-O/CZs. Although bulk Ni-Nb-O showed the comparable ethylene productivity with the Ni-Nb-O/CeO_2 and/or Ni-Nb-O/ZrO_2 at 400 ˚C, overall conversion of ethane into byproducts blocked the production of ethylene at 450 ˚C. This indicates that the bulk Ni-Nb-O has insufficient OSC at relatively high temperature because production of byproducts is related to the surface oxygen species that are generated by surface holes [41]. The reaction results clearly verified that the presence of $Ce_{0.3}Zr_{0.7}O_2$ (=CZ37) plays an important role for Ni-Nb-O toward the selective production of ethylene. Ni-Nb-O/CZ37 exhibited the highest level of ethylene production (6.3 μmol $g_{active\ cat}^{-1}$ s^{-1}) among the compared samples even though the Ni-Nb-O/CZ37 has the lowest surface area. The catalytic performance of the Ni-Nb-O/CZ37 was retained to 92% of initial rate formation of ethylene after 25 h (Fig. 2-12).

2.3.3 Electrochemical tests

As a more direct evidence for enhanced redox property of the Ni^{2+} in Ni-Nb-O/CZ37, cyclic voltammetry (CV) tests were performed under O_2-saturated condition and compared it with that of bulk Ni-Nb-O (Fig. 2-13). Apparent oxidation peaks at ~0.55 V (vs. Ag/AgCl) and reduction peaks at ~ 0.42 V (vs. Ag/AgCl) for both the Ni-Nb-O/CZ37 and bulk Ni-Nb-O were observed, while no pronounced redox peaks for $Ce_{0.3}Zr_{0.7}O_2$ (=CZ37) were obtained. These redox peaks are generated from the redox reaction of Ni atoms [61]. The sharper oxidation peak for Ni-Nb-O/CZ37 than that of bulk Ni-Nb-O indicates that the amount of redox participant (*i.e.*, Ni atoms) is larger in Ni-Nb-O/CZ37 than that in bulk Ni-Nb-O at given potential. This enlargement implies the increased amount of stoichiometric lattice oxygen during the redox reaction, which strongly enhances the ethylene selectivity [41]. Based on these experimental results, it is rational to infer that presence of $Ce_xZr_{1-x}O_2$ participates in the formation of reactive lattice oxygen species in Ni-Nb-O mixed oxide during the oxidation reaction. And this promotion effects for Ni-Nb-O should be attributed to the compensation of lattice oxygen from $Ce_xZr_{1-x}O_2$ into the oxygen vacancy sites, which leads to the enhancement in the ethylene selectivity.

Table 2-1. Nomenclature and physicochemical characteristics of the catalysts

Sample	Ce/Zr atomic ratio	Nb/Ni atomic ratio	Surface area (m^2 g^{-1})	Crystalline size of NiO[a] (nm)
Bulk Ni-Nb-O	-	0.176	61.8	20.2
Ni-Nb-O/CZ37	0.43		18.1	15.5
Ni-Nb-O/CZ55	1.00		24.6	14.1
Ni-Nb-O/CZ73	2.33		40.0	13.3

[a]Values were calculated by Scherrer equation.

Table 2-2. Lattice parameters of $Ce_{0.3}Zr_{0.7}O_2$ (=CZ37), $Ce_{0.5}Zr_{0.5}O_2$ (=CZ55), and $Ce_{0.7}Zr_{0.3}O_2$ (=CZ73).

Sample	$Ce_xZr_{1-x}O_2$ lattice parameter (Å)
$Ce_{0.3}Zr_{0.7}O_2$ (=CZ37)	5.218
$Ce_{0.5}Zr_{0.5}O_2$ (=CZ55)	5.393
$Ce_{0.7}Zr_{0.3}O_2$ (=CZ73)	5.410

Table 2-3. Selectivity of products for bulk Ni-Nb-O and Ni-Nb-O/CZ37 as a function of reaction temperature. Experiments were performed at 1 atm with a C_2H_6/O_2 molar ratio of 2:1 at the reactor inlet.

	Reaction temperature (˚C)	Selectivity of products (%)			
		C_2H_4	CO_2	CO	Others*
Bulk Ni-Nb-O	350	44.7	55.3	0	0
	400	41.7	58.3	0	0
	450	0	44.5	8.0	47.5
	500	-	-	-	-
Ni-Nb-O/CZ37	350	65.4	34.6	0	0
	400	61.3	38.7	0	0
	450	50.2	49.8	0	0
	500	0	33.8	27.1	39.1

*Products containing CH_4 and coke.

Table 2-4. Ethane conversion, ethylene selectivity, and ethylene productivity for the other samples. Experiments were performed at 1 atm and 450 ˚C with a C_2H_6/O_2 molar ratio of 2:1 at the reactor inlet.

Catalyst	Ethane conversion (%)	Ethylene selectivity (%)	Ethylene productivity ($\mu mol\ g_{active\ cat}^{-1}\ s^{-1}$)
CeO_2	5.2	18.9	0.04
ZrO_2	5.8	13.1	0.04
$Ce_{0.3}Zr_{0.7}O_2$ (=CZ37)	12.2	9.7	0.05
$Ce_{0.5}Zr_{0.5}O_2$ (=CZ55)	20.0	5.9	0.05
$Ce_{0.7}Zr_{0.3}O_2$ (=CZ73)	29.5	4.9	0.07

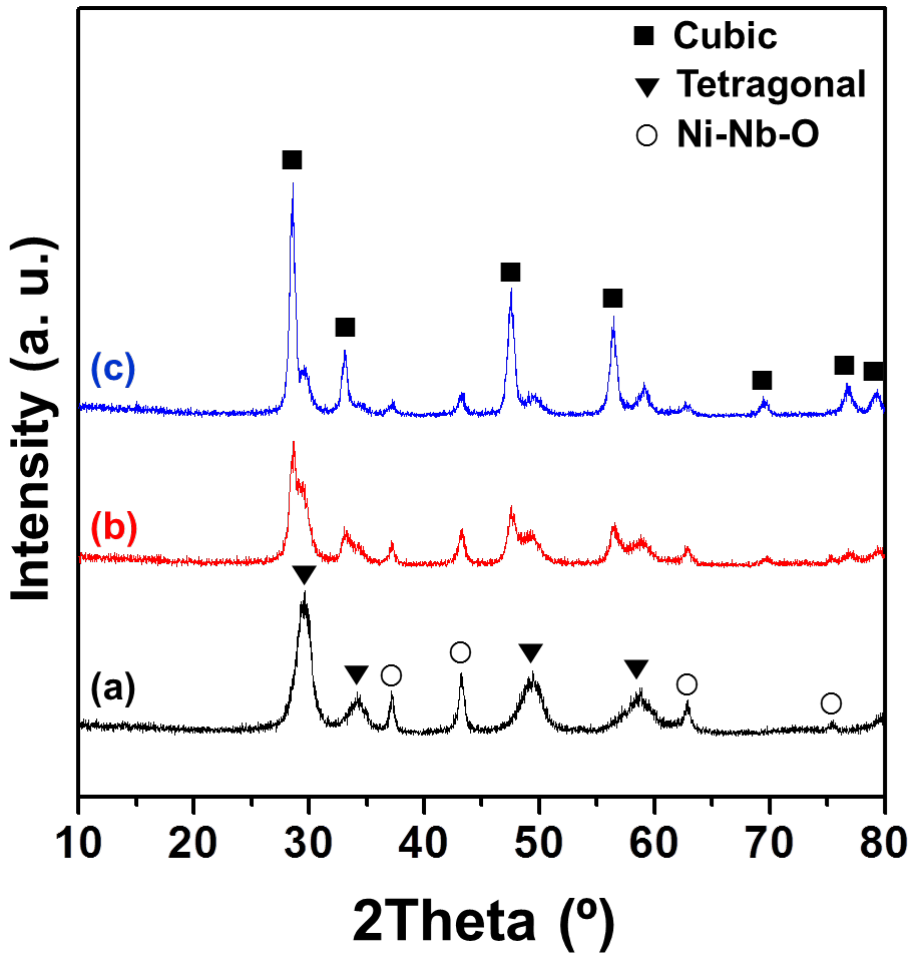

Fig. 2-1. XRD patterns of (A) (a) Ni-Nb-O/CZ37, (b) Ni-Nb-O/CZ55, and (c) Ni-Nb-O/CZ73.

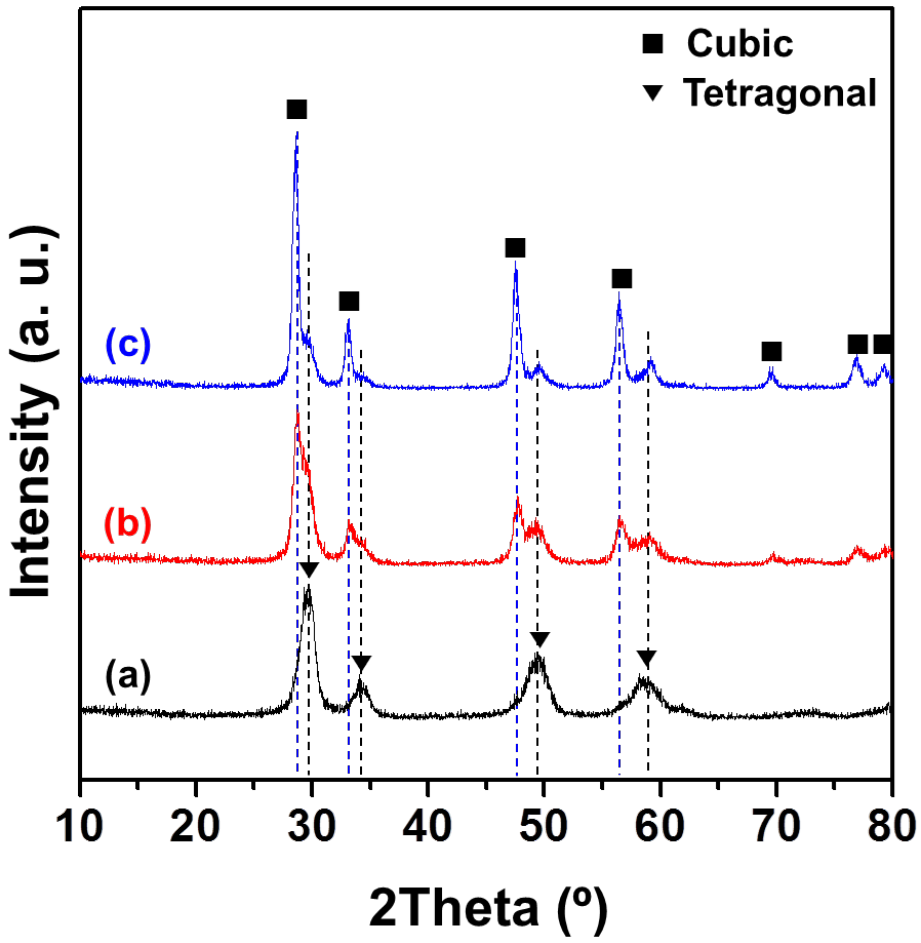

Fig. 2-2. XRD patterns of (a) CZ37, (b) CZ55, and (c) CZ73.

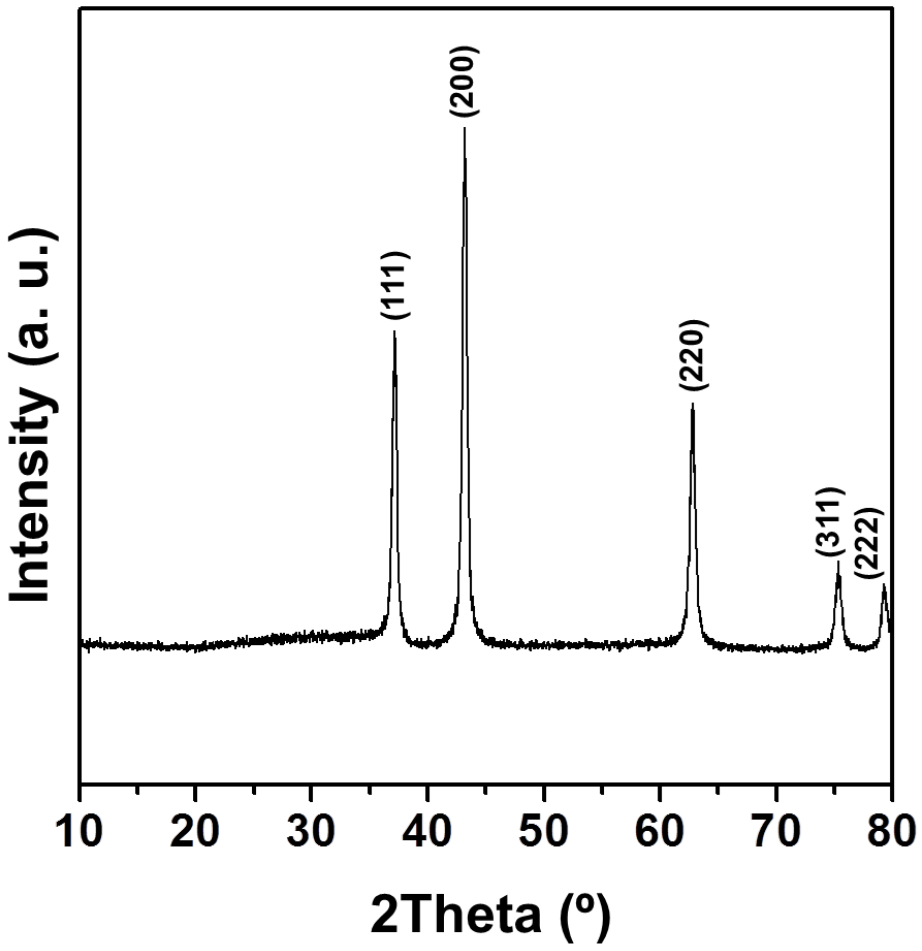

Fig. 2-3. XRD patterns of Ni-Nb-O.

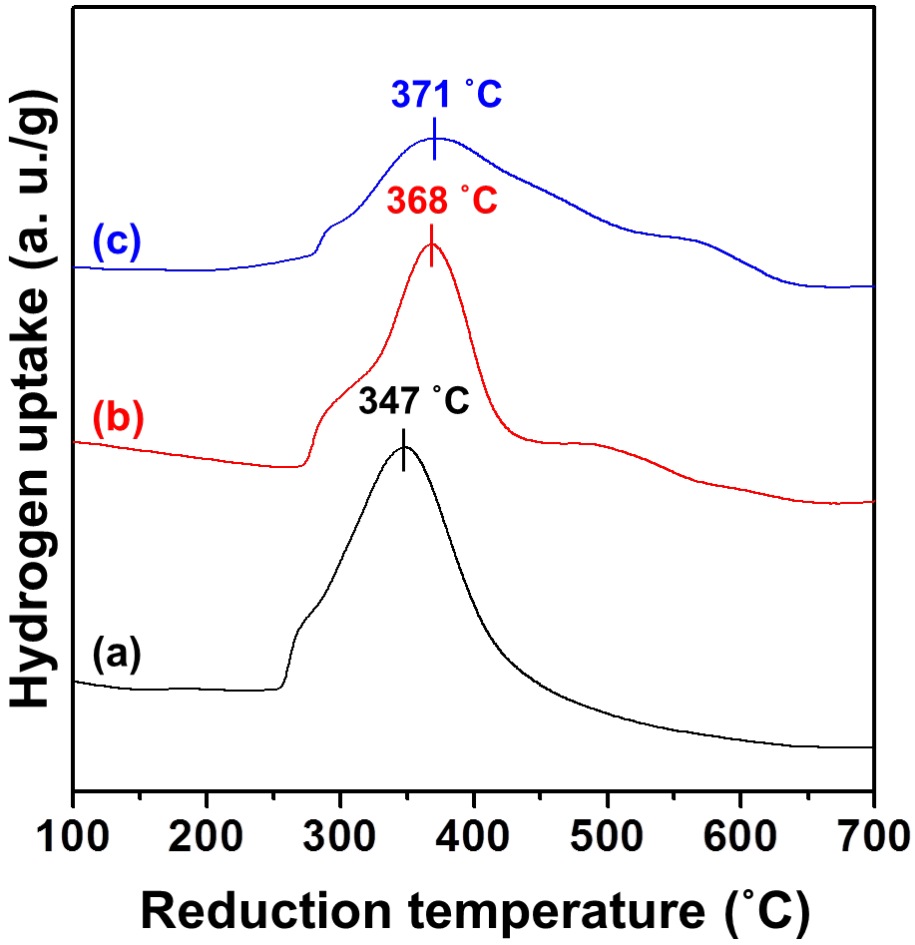

Fig. 2-4. H_2-TPR profiles of (a) Ni-Nb-O/CZ37, (b) Ni-Nb-O/CZ55, and (c) Ni-Nb-O/CZ73.

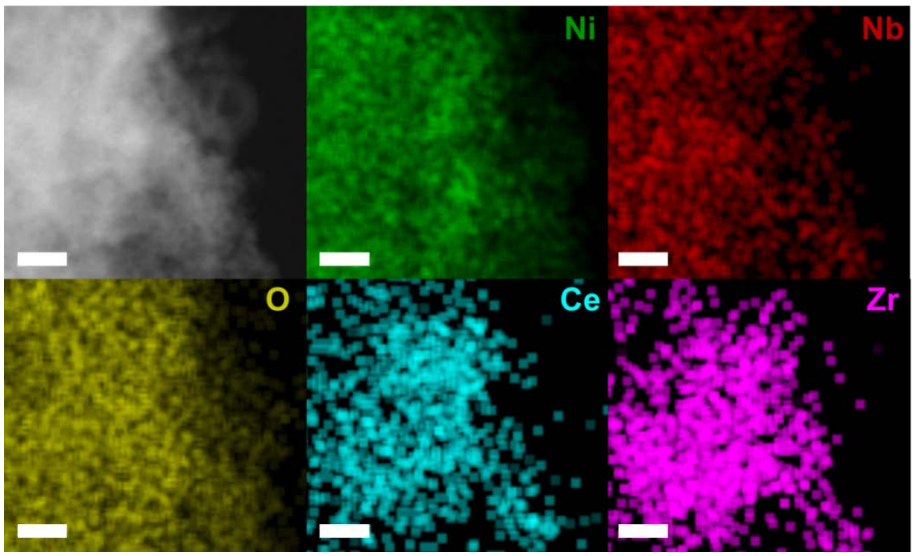

Fig. 2-5. HAADF-STEM images of Ni-Nb-O/CZ37 with elemental mapping of Ni, Nb, Ce, Zr, and O. Scale bars are 50 nm. (CZ37=$Ce_{0.3}Zr_{0.7}O_2$)

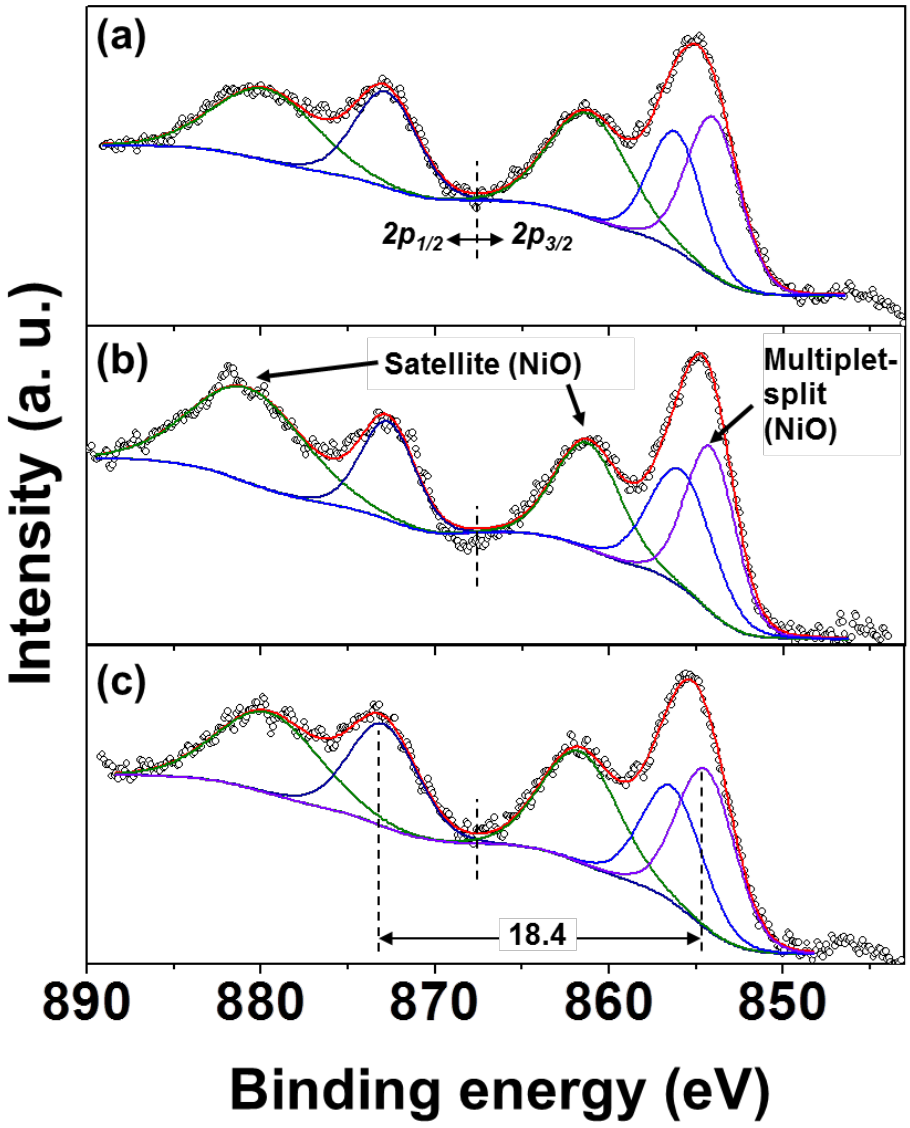

Fig. 2-6. XPS spectra of the Ni 2p core level for (a) Ni-Nb-O/CZ37, (b) Ni-Nb-O/CZ55, and (c) Ni-Nb-O/CZ73.

The analysis was fitted using the Shirley background and the fitted curves were deconvoluted based on both spin orbit coupling of the Ni and the Gaussian fitting. The Ni 2p spectra for Ni-Nb-O/CZs show five fitted peaks: $2p_{3/2}$ (854.4 eV) and its satellite (856.4 and 861.7 eV), $2p_{1/2}$ (872.9 eV) and its satellite (879.6 eV) [62,63]. The difference in the binding energies between Ni $2p_{1/2}$ and Ni $2p_{3/2}$ was measured at ~18.4 eV, indicating that the prepared Ni-Nb-O for Ni-Nb-O/CZs consists of the NiO structure [64,65].

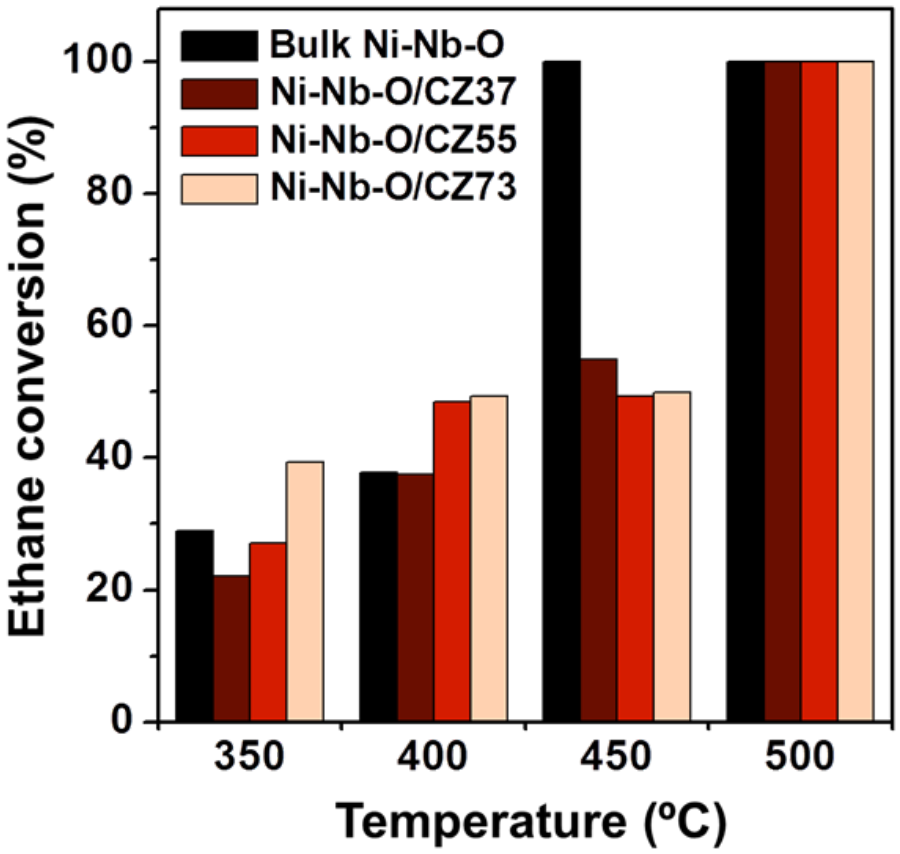

Fig. 2-7. Ethane conversion over bulk Ni-Nb-O, Ni-Nb-O/CZ37, Ni-Nb-O/CZ55, and Ni-Nb-O/CZ73. Experiments were performed at 1 atm with a C_2H_6/O_2 molar ratio of 2:1 at the reactor inlet.

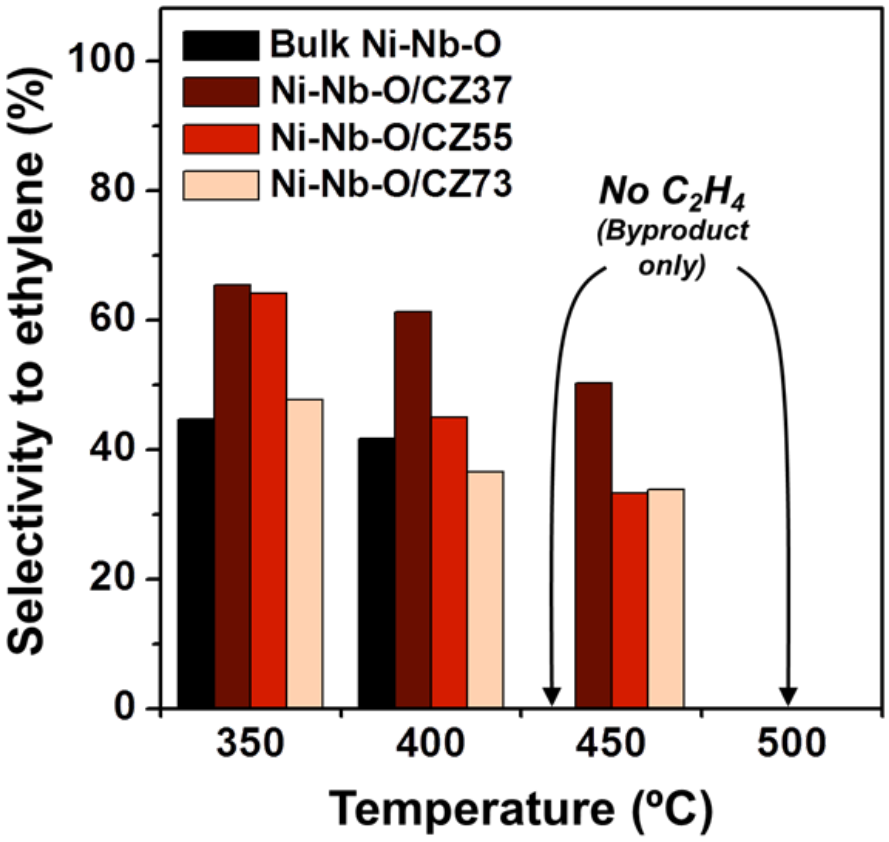

Fig. 2-8. Ethylene selectivity over bulk Ni-Nb-O, Ni-Nb-O/CZ37, Ni-Nb-O/CZ55, and Ni-Nb-O/CZ73. Experiments were performed at 1 atm with a C_2H_6/O_2 molar ratio of 2:1 at the reactor inlet.

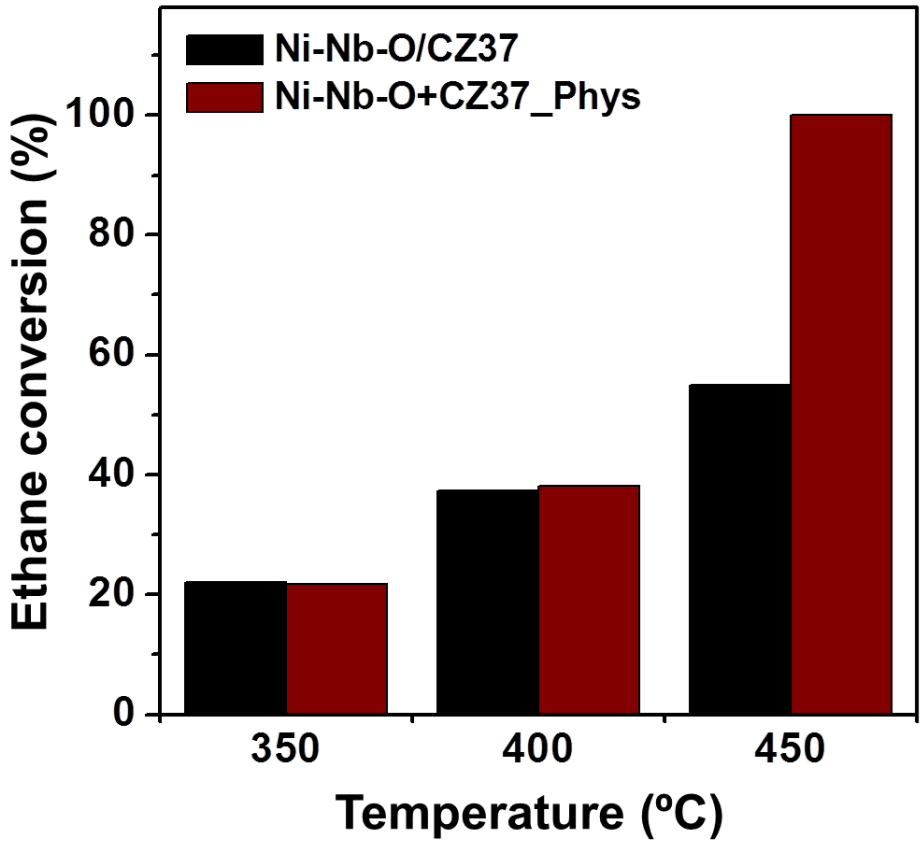

Fig. 2-9. Ethane conversion for Ni-Nb-O/CZ37 and physically mixed Ni-Nb-O + CZ37. Experiments were performed at 1 atm with a C_2H_6/O_2 molar ratio of 2:1 at the reactor inlet.

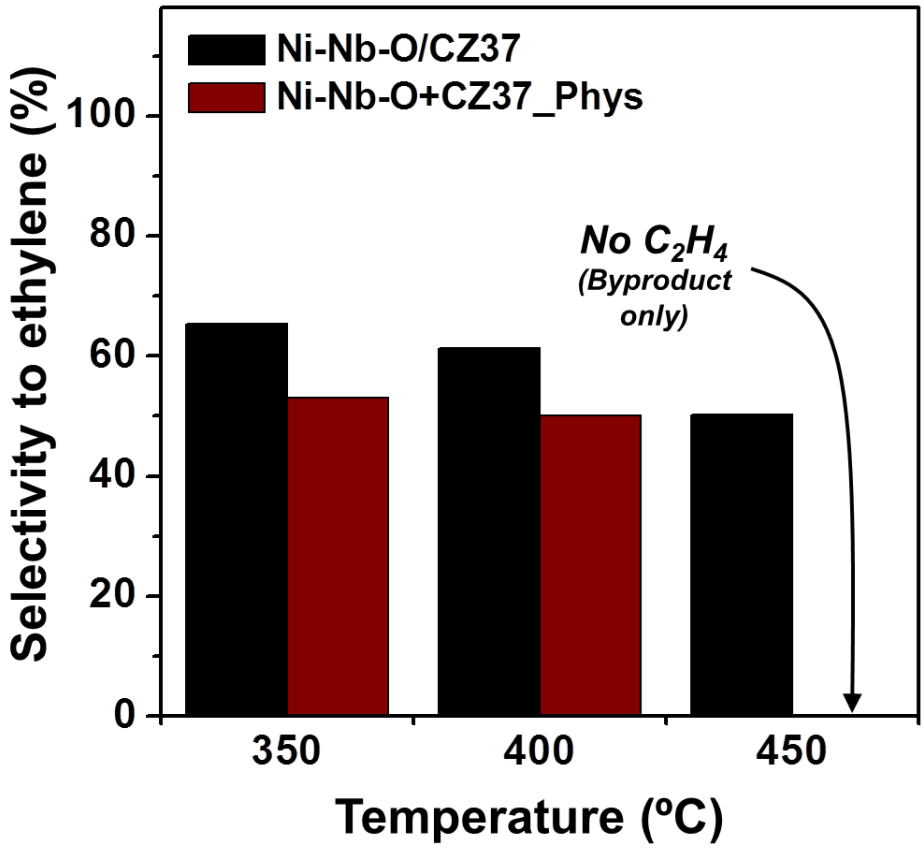

Fig. 2-10. Ethylene selectivity for Ni-Nb-O/CZ37 and physically mixed Ni-Nb-O + CZ37. Experiments were performed at 1 atm with a C_2H_6/O_2 molar ratio of 2:1 at the reactor inlet.

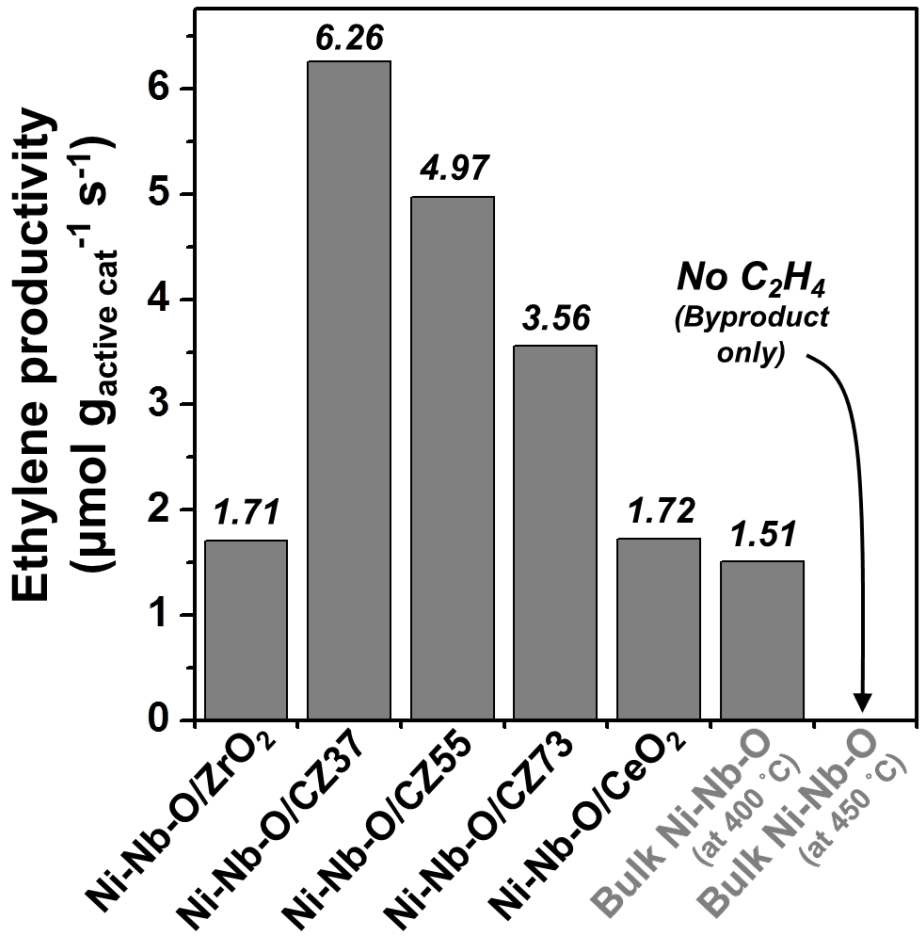

Fig. 2-11. Productivity of ethylene over Ni-Nb-O/ZrO_2, Ni-Nb-O/CeO_2, Ni-Nb-O/CZ37, Ni-Nb-O/CZ55, Ni-Nb-O/CZ73, and bulk Ni-Nb-O. The resultant data-sets were obtained at 450 ˚C for Ni-Nb-O/ZrO_2, Ni-Nb-O/CeO_2, and Ni-Nb-O/CZs. For better comparison, data-sets for bulk Ni-Nb-O were obtained at both 400 and 450 ˚C. Experiments were performed at 1 atm with a C_2H_6/O_2 molar ratio of 2:1 at the reactor inlet.

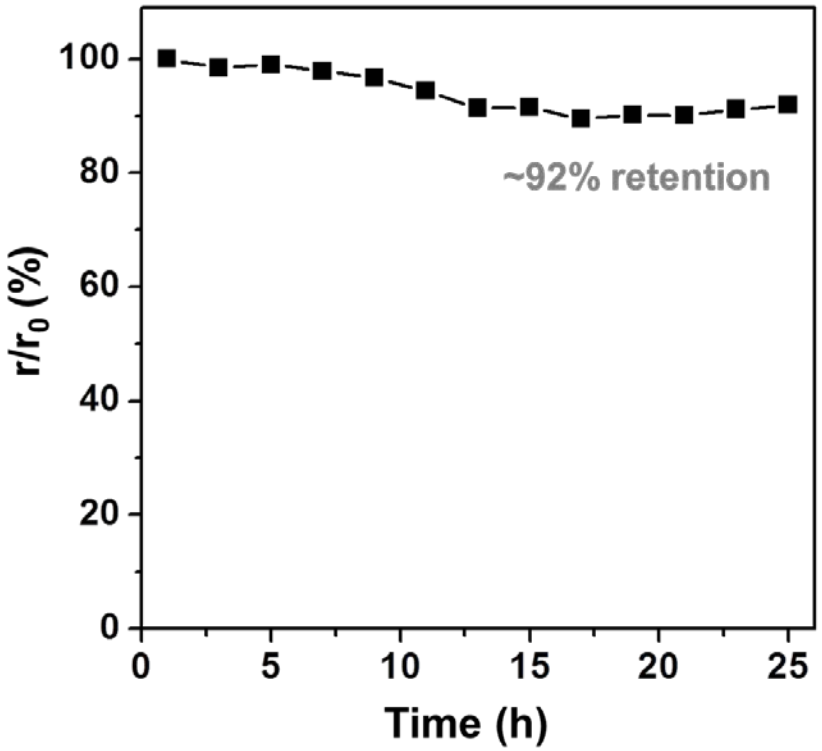

Fig. 2-12. Catalytic life of Ni-Nb-O/CZ37 at 450 ºC for 25 h. Experiments were performed at 1 atm with a C_2H_6/O_2 molar ratio of 2:1 at the reactor inlet. "r" is the rate of ethylene formation and "r_0" is the initial rate of ethylene formation.

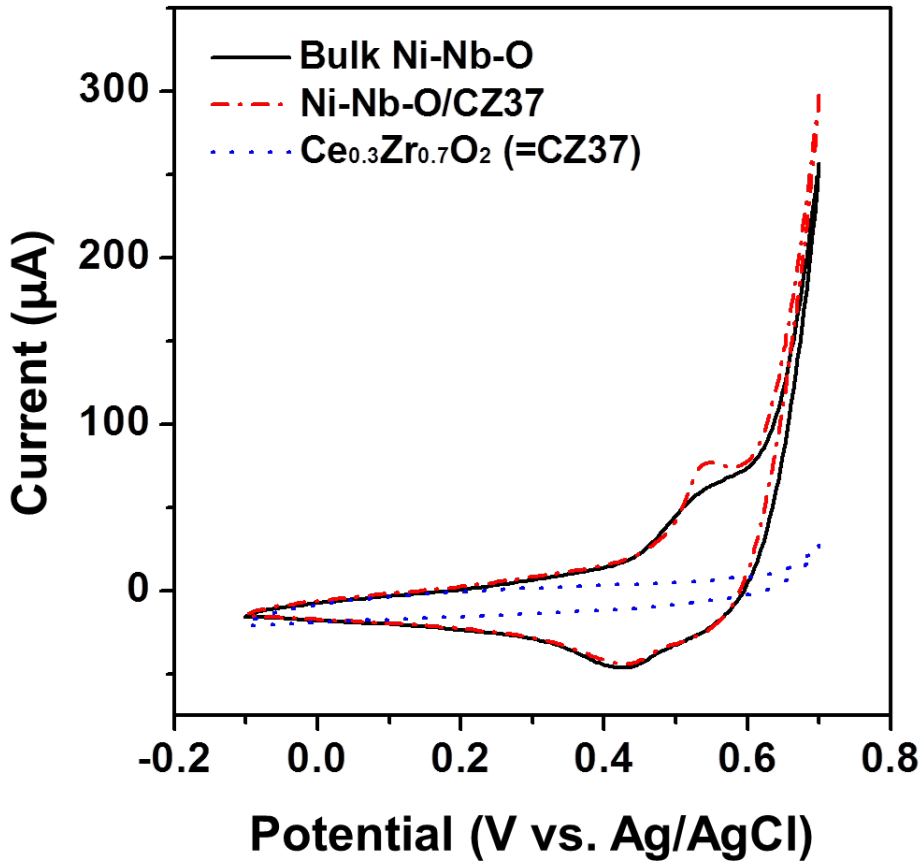

Fig. 2-13. Results of cyclic voltammetry tests for bulk Ni-Nb-O, Ni-Nb-O/CZ37, and $Ce_{0.3}Zr_{0.7}O_2$.

Chapter 3. Development of Ce-doped MoVTeNbO catalyst for low temperature oxidative dehydrogenation of ethane with almost 100% ethylene selectivity

3.1 Introduction

Molybdenum-Vanadium (Mo-V) containg mixed metal oxides have intensively been studied as an efficient catalyst with high ethylene yields for oxidative dehydrogenation of ethane (ODHE) reaction at low reaction temperature [66-74]. Importantly, these catalysts can be improved in terms of ethylene selectivity and productivity by incorporation of heteroatoms. As an attempts to further develop Mo-V catalyst, insertion of Tellurium (Te) and niobium (Nb) into the lattice structure of Mo-V, that is, MoVTeNbO mixed oxide, has been spotlighted because the significant improvement of characteristics for active sites can be achieved [66]. The active phase of the MoVTeNbO catalysts, called *M1*, is a solid solution that can selectively produce ethylene than that of *M2* [66].

Despite the success in the aspet of improving catalytic performance, there is still lack of ethylene selectivity at high reaction temperature which energetically enhances catalytic activity. This limitation is derived from the formation of several byproducts (*e.g.*, CO_x) at high reaction temperature,

which impedes an increase in production rate of ethylene and requires additional separation process in the output of the reactor. On the other hands, catalytic activity decreases at low reaction temperature, resulting in the decrease in ethylene productivity [66-68]. These observations imply that other improvement strategies have to be explored to design a MoVTeNbO catalyst exhibiting high catalytic activity with excellent ethylene selectivity at low reaction temperature.

Strategies for proper solving these issues should target their fundamental origins. The reaction pathway for the ODHE reaction on MoVTeNbO mixed oxide is governed by the Mars-van Krevelen mechanism, which consumes lattice oxygen within the catalyst to produce ethylene [44]. In order to enhance the catalytic activity, better reflux of lattice oxygen is required because it is believed that the lattice oxygen plays a role of active site for the production of ethylene [68]. Therefore, introduction of additional heteroatom into MoVTeNbO showing excellent oxygen storage and release capacity (OSC), cerium (Ce), for example, can be a promising strategy to achieve aforementioned strategy.

In this study, we report on a development of Ce-doped MoVTeNbO composites as an efficient catalyst for the production of ethylene via ODHE reaction. For the optimization of the composite, Ce atoms were introduced to MoVTeNbO with various concentrations, with maintaining active *M1* phase. The role of Ce dopant was suggested by physicochemical characterizations, in details, qualification and quantification of lattice oxygen through electrochemical tests and pulse MS method, respectively. Main objective

focuses on the enhancement in ethylene productivity even at low reaction temperature (350-400 ˚C) using Ce-doped MoVTeNbO catalyst, compared to conventional MoVTeNbO.

3.2 Experimental

3.2.1 Preparation of catalysts

A series of Ce-doped MoVTeNbO catalysts were prepared using the hydrothermal method previously described [75]. At first, specific amounts of ammonium molbdate, vanadyl sulfate, telluric acid and cerium nitrate in proportion leading to the ratio: Mo/V/Te/Nb = 1/0.2/0.17/0.17 and Ce contents are varied with 0.05, 0.1, 0.2, and 0.3 in their ratio. Mo, V, Te, and Ce precursors are first dissolved in deionized (DI) water together and heated to 80 ˚C under vigorous stirring (solution A). In parallel, an aqueous solution containing niobium oxalate and oxalic acid was also prepared at 80 ˚C (solution B). The color of "solution A" is sequentially changed from dark purple, green, and to yellow. After cooling the solution A and B to room temperature, "solution B" is slowly added to the "solution A" under vigorous stirring. This mixture was placed in a teflon-lined autoclave and heated at 175 °C for 48 hours to form a Ce-doped MoVTeNbO composite. The precipitate was isolated by centrifugation at 10,000 rpm for 10 min and washed several times with DI water to remove residual ions. After drying at 60 °C for 12 hours, *M1* phase Ce-doped MoVTeNbO was obtained by calcination at 600 °C for 2 hours under N_2 atmosphere.

3.2.2 Characterizations

An X-ray diffractometer (XRD, Rigaku, D/max-2500/PC) using Cu Kα radiation (wavelength = 0.154 nm) as an incident beam at 50 kV and 100 mA was utilized to confirm the crystalline size and elemental phases of the prepared composites. The shapes and microstructures of the synthesized Ce-doped MoVTeNbO composites were characterized by high-resolution transmission electron microscopy (HR-TEM, JEM 3010-JEOL, 300 kV). N_2 adsorption-desorption isotherms were measured with a Micromeritics ASAP 2010 instrument. The Brunauer-Emmett-Teller (BET) method was utilized to calculate the specific surface area.

3.2.3 Catalytic reaction test

The oxidative dehydrogenation (ODH) of ethane was performed in a fixed bed reactor (a quartz tube with 8 mm i.d. and a length of 290 mm). The reaction temperature was varied from 350 to 500 °C under atmospheric pressure. A thermocouple was installed at the outer surface of the reactor near the catalyst bed in order to measure the reaction temperature. The gas feed consisted of $C_2H_6/O_2/He/N_2$ with a 10/5/60/25 molar ratio at a total flow rate of 20 cm^3 min^{-1}. The used amount of catalyst was 0.2 g. He and N_2 gases were used as an inert gas and an internal standard gas, respectively.

The reactants and products were analyzed using an on-line gas chromatograph (GC, ACME 6100, Younglin Instrument) equipped with both a flame ionization detector (FID) and a thermal conductivity detector (TCD). The FID was used for a more precise detection of hydrocarbons. Two

columns were used in the analysis, a Porapak Q (CO_2, C_2H_4, C_2H_6) and a Molsieve 13X (N_2, O_2, CO). The ethane conversion and ethylene selectivity were defined on a carbon basis. The acquired experimental data were calculated using the following equations:

$$X_{C_2H_6} = \frac{f_{C_2H_6\,(in)} - f_{C_2H_6\,(out)}}{f_{C_2H_6\,(in)}} \times 100\ (\%) \quad (1)$$

$$S_{C_2H_4} = \frac{f_{C_2H_4\,(out)}}{f_{C_2H_6\,(in)} - f_{C_2H_6\,(out)}} \times 100\ (\%) \quad (2)$$

where $X_{C_2H_6}$ is the ethane conversion, $S_{C_2H_4}$ is the selectivity to ethylene, and f is the molar flow rate in the effluent gas. For each test, the detected chemical mixture with C_2H_6, C_2H_4, and CO_2 gives an almost close carbon balance of 100%. CH_4 and CO were not detected under our measurement conditions.

3.3 Results and discussion

3.3.1 Effect of heat treatment under nitrogen after *M2* phase dissolution

The results of the structural phases for Ce(0.1)-doped MoVTeNbO after heat treatment with varying the calcination temperature from 500 °C to 700 °C are presented in Fig. 3-1. It has clearly seen that the crystallinity of the catalyst heat treated at 500 °C is much lower than those of them treated at 600, 650, and 700 °C. As the calcination temperature increased from 600 °C to 700 °C, peak intensity corresponding to *M1* phase decreased. It is noteworthy that the optimum calcination temperature for Ce(0.1)-doped MoVTeNbO is 600 °C, denoted herein as Ce(0.1)-doped MoVTeNbO_600, based on the previous results that the *M1* is the active phase to convert ethane molecule to ethylene selectively. To confirm that having large amount of *M1* phase is one of the key parameters for determination of the ethylene production ability, ODHE reaction tests were conducted for Ce(0.1)-doped MoVTeNbO samples prepared as a function of activation temperature as shown in Fig. 3-2. In a simple comparison for ethylene yields, Ce(0.1)-doped MoVTeNbO_600 exhibited the highest ethylene yield for all reaction temperatures among the prepared samples. Interestingly, the ethylene production ability of Ce(0.1)-doped MoVTeNbO_650 and Ce(0.1)-doped MoVTeNbO_700 were inferior to that of the Ce(0.1)-doped MoVTeNbO_500 until reaching 375 °C. This should be attributed to the presence of M2 phase for the Ce(0.1)-doped MoVTeNbO_650 and Ce(0.1)-

doped MoVTeNbO_700 samples. Thus, it seems that the removal of M2 phase is more crucial than the presence of M1 phase for enhancement in the ethylene productivity. It should be noted that the level of ethylene yield (50-60 %) at around 350 ℃ for as-prepared catalysts are comparable to previously reported results, indicating that the evaluation of effects of Ce dopant is relevant and acceptable [66-70].

3.3.2 Effect of Ce doping amount

Another factor that could influences on the formation of structural phase is the amount of Ce dopant. Excess substritutional doping of guest atoms into the host material usually leads to the distortion of overall lattice structure, which confers the mother structure to have labile characteristics. As a result, the host material can be converted into the more stable form than the intact one. The changes in the lattice structure and/or the phase of the host material would strongly influence on the catalytic performance, and thus, investigation of optimum amount of dopant is important without losing its original crystal formation. The amount of Ce dopant was varied with 0.05 to 0.3 mol% within the Ce-doped MoVTeNbO composites. XRD patterns for the controlled samples are shown in Fig. 3-3. In overall, crystallinity of samples was maintained, or somehow increased, when Ce heteroatom was incorporated into the MoVTeNbO composite. It was observed that the intensity of the representative peak corresponding to *M1* phase at around 20 ° (2 theta) gradually increased until the Ce(0.1)-doped MoVTeNbO at the low

doping level, whereas the intensity decreased back after the Ce(0.2)-doped MoVTeNbO at the high doping level. Finally, the peak was disappeared for Ce(0.3)-doped MoVTeNbO samples, indicating that the catalytic activity for Ce(0.3)-doped MoVTeNbO will be lower than those of other samples due to the degradation of active sites. Moreover, the peak intensity corresponding to the *M2* phase tended to increase as the doping amount of Ce increased. These results imply that the optimum amount of Ce dopant should be 0.1 for maximizing the ethylene production.

The shape, size and the lattice structures of the Ce(0.2 and 0.3, respectively)-doped MoVTeNbO samples were investigated by transmission electron microscopy (TEM) and compared with that of pure MoVTeNbO, as shown in Fig. 3-4. Both of the undoped and Ce(0.2)-doped samples showed that the particle shapes were rod-like features and the length of them were around ~50 μm. Otherwise, the shape of Ce(0.3)-doped MoVTeNbO particles were obviously irregular, compared to those of undoped and Ce(0.2)-doped MoVTeNbO. The d-space of (110) for MoVTeNbO and MoVTeNbCe(0.2)O were examined to be similar each other, 18.77 and 17.43 Å, respectively, whereas the one for the MoVTeNbCe(0.3)O was quite narrow, 3.17 Å (Fig. 3-5, 3-6, and 3-7). This difference in the d-space values might be ascribed to the dissolution of M1 phase in Ce(0.3)-doped MoVTeNbO, which is in good agreement with the results obtained from XRD analyses (Fig. 3-3). Therefore, the effects of Ce amount on the structural and/or phase changes can be explained that the excess amount of Ce dopants can collapse and/or change them and the atoms are

substitutionally doped in the lattice structure of MoVTeNbO. Because the intact structure of MoVTeNbO should be well-maintained when the presence of other incorporation features of Ce atoms, such as deposition of Ce clusters on the MoVTeNbO surface, is taken place.

To examine the catalytic performance with varying the amount of Ce dopants in MoVTeNbO, ODHE reaction tests were conducted with respect to the reaction temperature range from 250 to 325 °C, as shown in Fig. 3-8. Ce(0.1)-doped MoVTeNbO exhibited higher ethylene yield (~26 %) than those of Ce(0.05)-doped MoVTeNbO (~19 %), Ce(0.3)-doped MoVTeNbO (~0 %), and pure MoVTeNbO (~19%) at 235 °C. This tendency is in good agreement with the expectations obtained from aforementioned XRD and TEM analyses that *M1* structure is active phase for the production of ethylene via ODHE process. In particular, all samples showed almost 100% ethylene selectivity, which indicates that the catalytic activity increased with respect to the amount of Ce dopants. In 2012, A. Trunschke *et al*. reported that the treatment of MoVTeNbO with H_2O_2 results in the dissolution of *M2* phase, which does have merits in the development of *M1* phase oriented MoVTeNbO [76]. In order to increase the phase ratio of *M1*/*M2*, H_2O_2 treatment of Ce(0.1)-doped MoVTeNbO catalyst was conducted, denoted herein as Ce(0.1)-doped MoVTeNbO_H_2O_2 as reported previously and the catalytic performance of it was examined. The results showed that the reaction temperature for Ce(0.1)-doped MoVTeNbO_H_2O_2 was highly reduced ($\Delta T=50\pm10$ °C), compared to the purd MoVTeNbO under identical value of ethylene yield. It should be noted that that the specific surface areas

for all prepared samples were very similar (50±5 m^2 g^{-1}), indicating that the effects of exposed surface area on catalytic activity can be negligible. Therefore, we concluded that the incorporation of Ce atoms greatly enhances the catalytic activity without losing its ethylene selectivity.

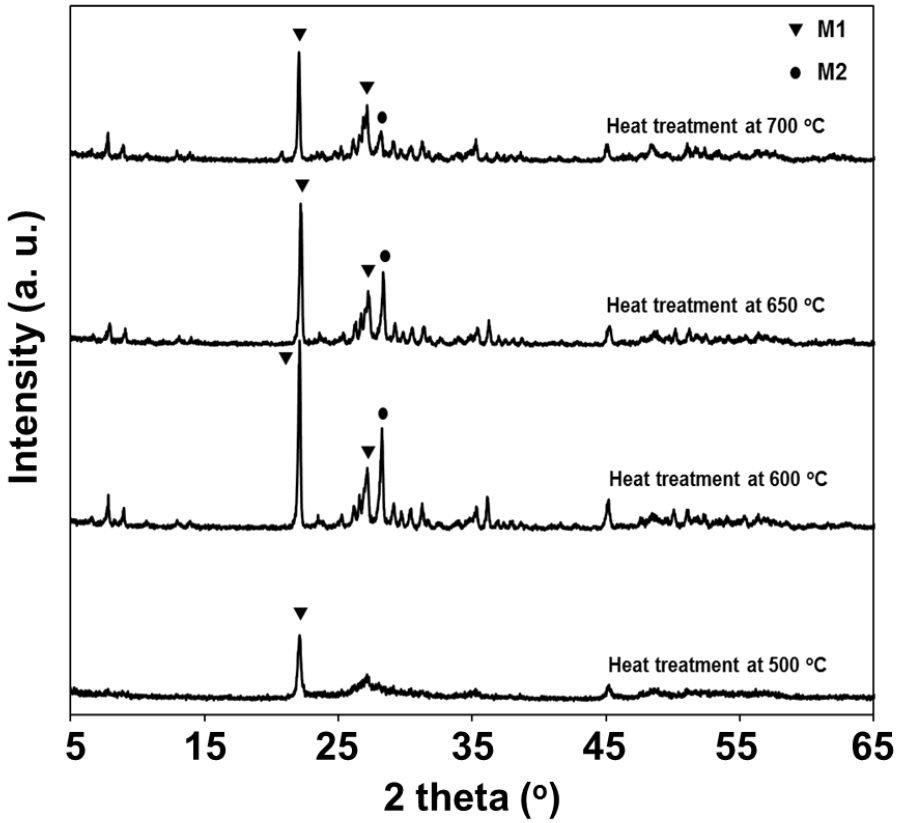

Fig. 3-1. XRD patterns of Ce(0.1)-doped MoVTeNbO after heat treatment at different temperatures.

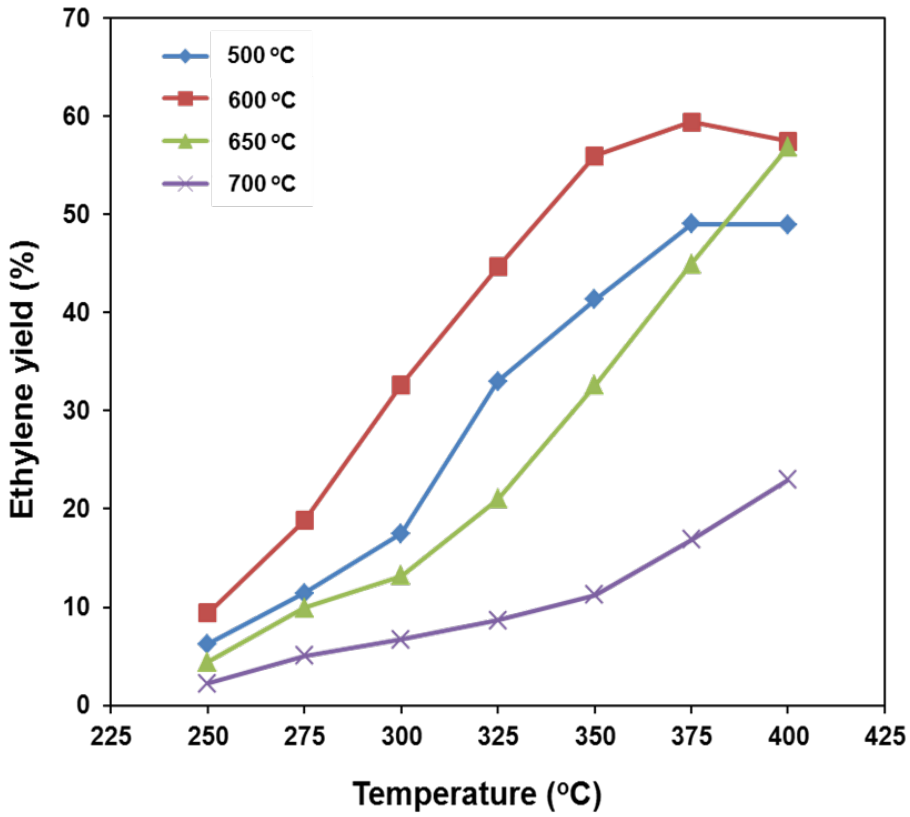

Fig. 3-2. Ethylene yield over Ce(0.1)-doped MoVTeNbO catalysts after heat treatment under N_2 stream at different temperatures. 0.2 g catalyst and 20 mL min^{-1} of total flow rate. 0.5 of C_2H_6 to O_2 molar ratio.

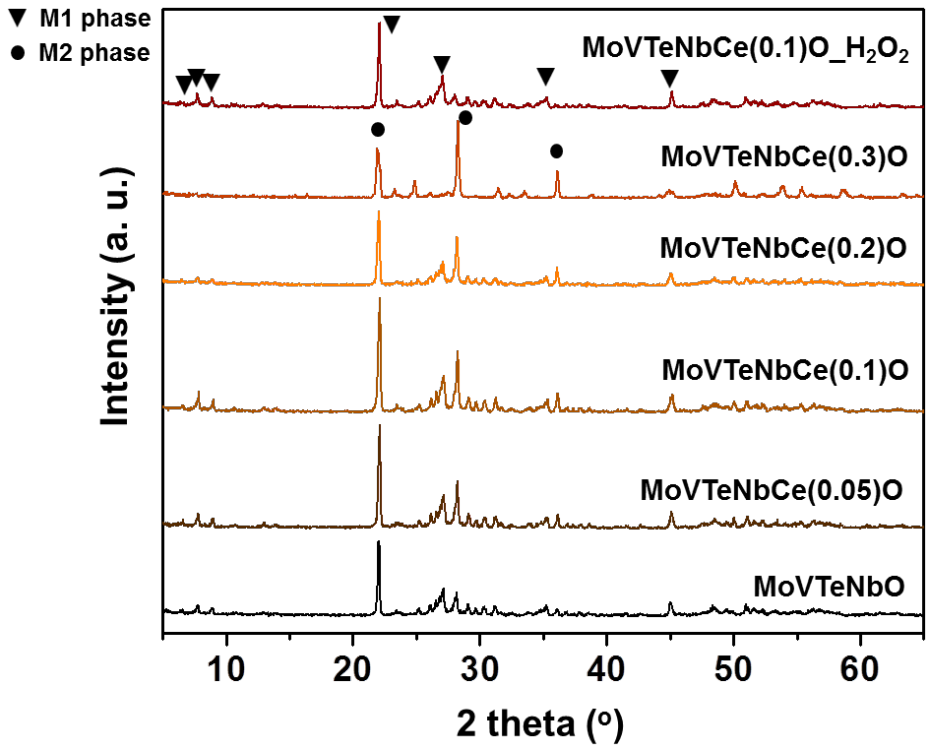

Fig. 3-3. XRD patterns of MoVTeNbO and Ce-doped MoVTeNbO catalyst with different Ce ratio after heat treatment (600 °C).

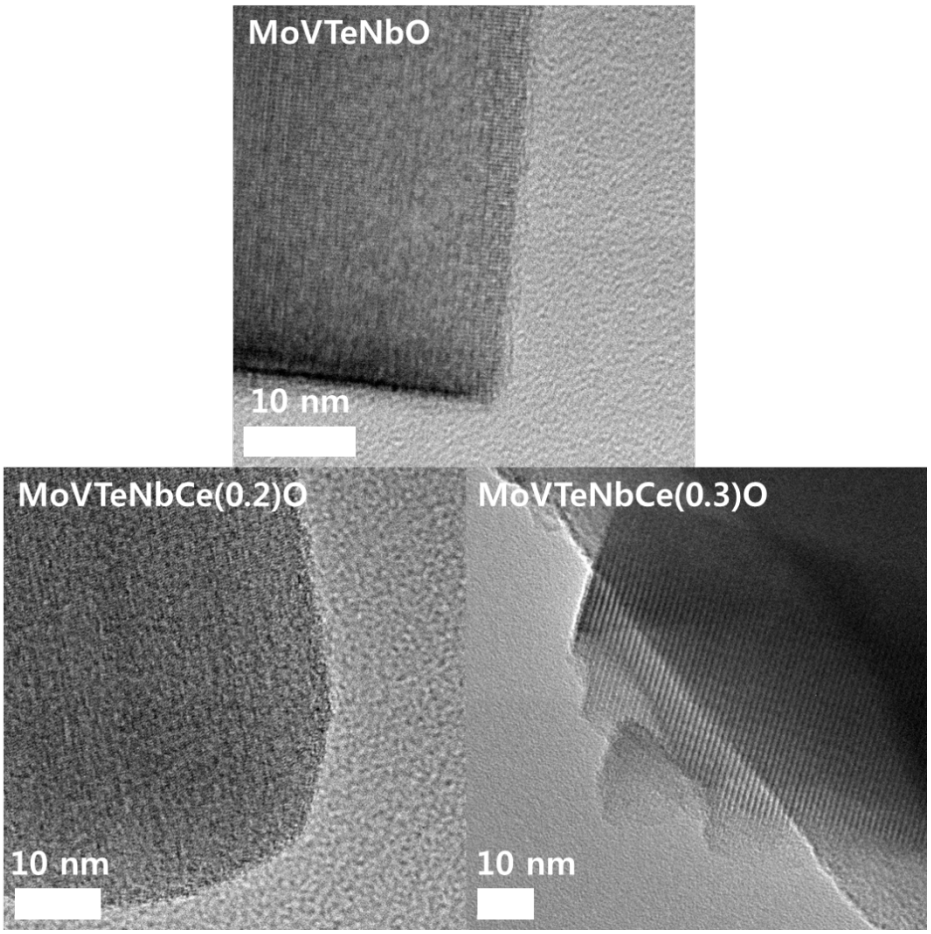

Fig. 3-4. TEM images of MoVTeNbO and Ce-doped MoVTeNbO catalyst with different Ce ratio after heat treatment (600 °C).

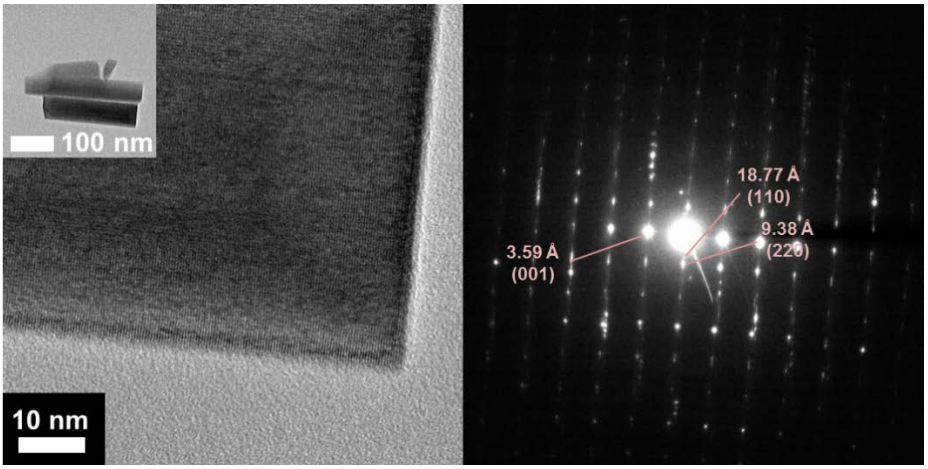

Fig. 3-5. TEM images and saed pattern of MoVTeNbO.

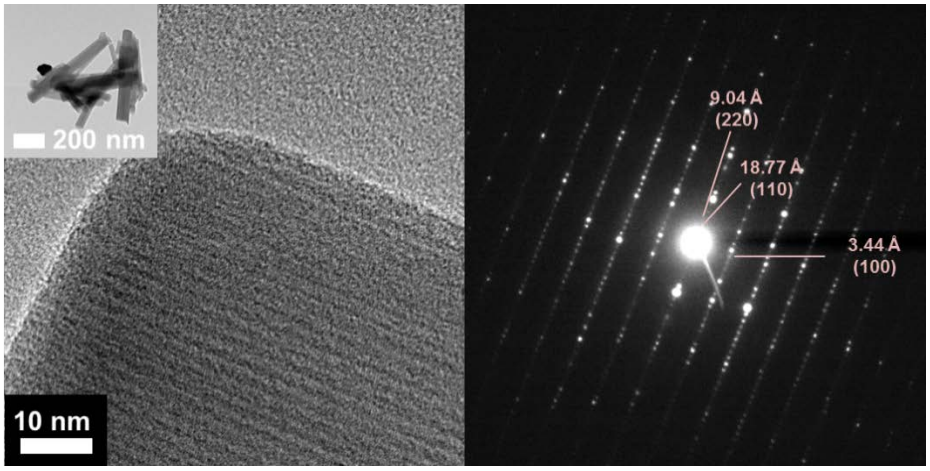

Fig. 3-6. TEM images and saed pattern of MoVTeNbCe(0.2)O.

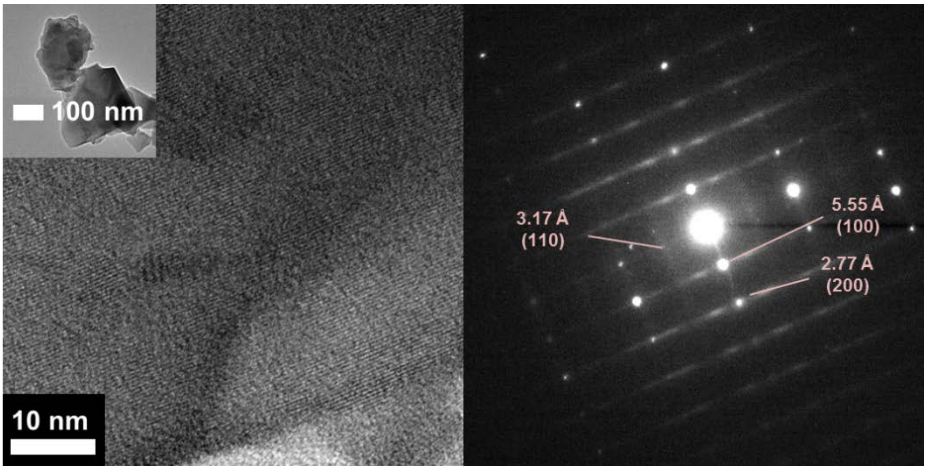

Fig. 3-7. TEM images and saed pattern of MoVTeNbCe(0.3)O.

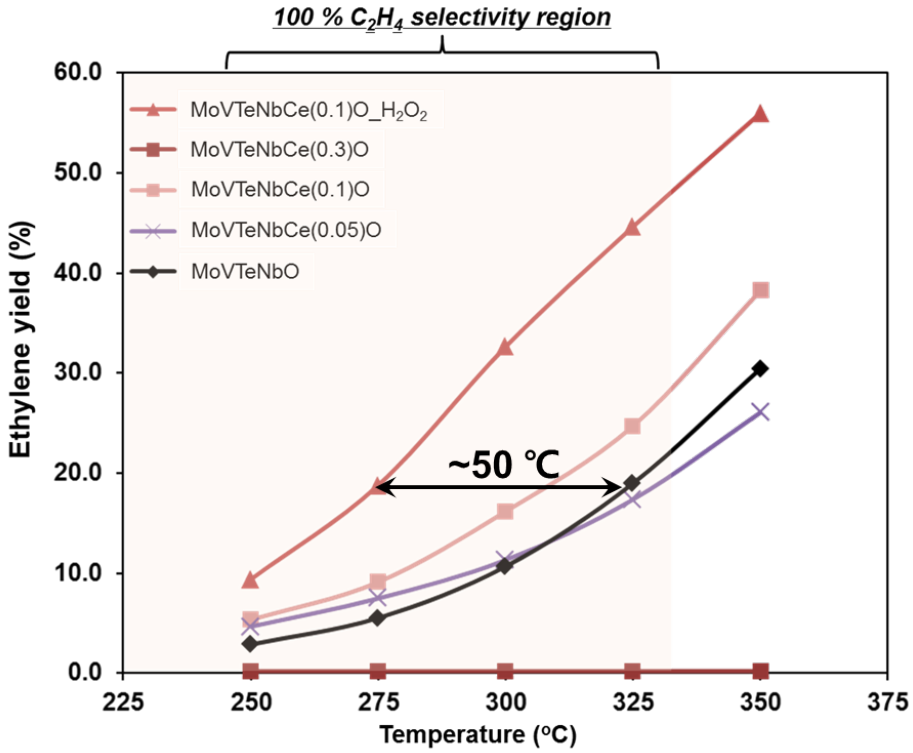

Fig. 3-8. Ethylene yield of MoVTeNbO and Ce-doped MoVTeNbO catalysts with different Ce contents for ODHE.

Chapter 4. Summary and Conclusions

As one of the strategies for enhancing redox property of NiO based catalyst for use in oxidative dehydrogenation of ethane, namely ODHE, Ni-Nb-O/$Ce_xZr_{1-x}O_2$ composite was proposed in Chapter 2. One of the key parameters in designing desirable physicochemical property of Ni-Nb-O for use in ODHE catalyst is the sufficient reflux of lattice oxygen within the catalyst, based on the Mars-van Krevelen mechanism. Introduction of such a material, $Ce_xZr_{1-x}O_2$, having excellent oxygen storage and storage capability (OSC) to the Ni-Nb-O active catalyst enhanced the redox property of Ni-Nb-O, resulting in the enhanced ethylene selectivity. Furthermore, this promotion effects allowed Ni-Nb-O catalystic system to be operational at relatively high reaction temperature, exhibiting high level of ethane conversion. Results of electrochemical tests and relevant control tests proved that the introduction of $Ce_xZr_{1-x}O_2$ material reduces the amount of nonstoichiometric Ni^{2+}, which led to the increased amount of nucleophilic lattice oxygen in Ni-Nb-O catalyst. Consequently, 6 times higher ethylene productivity can be achieved using this external promotion strategy.

As one of the other strategies for tuning the active sites of catalyst for use in ODHE process, doping technique was introduced with Ce heteroatoms into MoVTeNbO composite, namely Ce-doped MoVTeNbO. Activation temperature (*i.e.*, heat treatment) was optimized to maximize *M1* phase, which is an active site for selective production of ethylene rather than the byproducts such as CO_x and/or CH_4. And the doping amount of Ce was also

optimized to be 0.1% of molar ratio within Ce-doped MoVTeNbO, based on the *M1*/*M2* ratio. The results of reaction tests proved that the presence of *M1* phase with high crystallinity in MoVTeNbO composite is very important to produce ethylene with its selectivity around 100 %. Results of XRD patterns and TEM images confirmed that the excess doping of Ce heteroatom into MoVTeNbO leads to the distortion of its lattice structure and subsequent transfer into *M2* phase. The effects of H_2O_2 treatment was also investigated for the Ce(0.1)-doped MoVTeNbO in order to maximize the *M1*/*M2* phase again. The final form of *M1* phase Ce(0.1)-doped MoVTeNbO exhibited significantly high catalytic performance that the catalyst exhibited comparable ethylene yield at almost 50 °C lower reaction temperature than that of the pure MoVTeNbO catalyst.

Bibliography

[1] H. Zimmermann, R. Walzl, in Ullmann's Encyclopedia of Industrial Chemistry, Wiley-VCH, Weinheim, 2000.

[2] Z. Skoufa, G. Xantri, E. heracleous, A.A. Lemonidou, Appl. Catal. A: Gen. 2014, 471, 107.

[3] S. Deng, H. Li, S. Li, Y. Zhang, J. Mol. Cat. A: Chem. 2007, 268, 169.

[4] C. Liu, U. S. Ozkan, J. Mol. Cat. A: Chem. 2004, 220, 53.

[5] J. P. Bortolozzi, L. B. Gutierrez, M. A. Ulla, Catal. Commun. 2014, 43, 197.

[6] H. H. Kristoffersen, H. Metiu, J. Phys. Chem. C 2015, 119, 8681.

[7] G.-L. Dai, Z.-P. Liu, W.-N. Wang, J. Lu, K.-N. Fan, J. Phys. Chem. C 2008, 112, 3719.

[8] R. Koirala, R. Buechel, F. Krumeich, S. E. Pratsinis, A. Baiker, ACS Catal. 2015, 5, 690.

[9] E. W. McFarland, H. Metiu, Chem. Rev. 2013, 113, 4391.

[10] G. Che-Galicia, R. Quintana, Solórzano, R. S. Ruiz-Martínez, J. S. Valente, C. O. Castillo-Araiza,

[11] F. Rahman, K. F. Loughlin, M. A. Al-Saleh, M. R. Saeed, N. M. Tukur, M. M. Hossain, K. Karim, A. Mamedov, Appl. Catal. A: Gen. 2010, 375, 17.

[12] S. Mao, B. Li, D. Su, J. Mater. Chem. A 2014, 2, 5287.

[13] M. M. Bhasin, J. H. McCain, B. V. Vora, T. Imai, P. R. Pujado, Appl. Catal. A: Gen. 2001, 221, 397.

[14] F. Cavani, F. Trifiro, Catal. Today 1999, 51, 561.

[15] J. A. Lercher, F. N. Naraschewski in Nanostructured Catalysts-Selective Oxidations, Royal Society of Chemistry, Cambridge, 2011, pp. 5.

[16] E. A. Mamedov, V. Cortes Corberan, Appl. Catal. A: Gen. 1995, 127, 1.

[17] R. Grabowski, Catal. Rev. Sci. Eng. 2006, 48, 199.

[18] E. M. Thorsteinson, T. P. Wilson, F. G. Young, P. H. Kasai, J. Catal. 1978, 52, 116.

[19] R. B. Watson, S. L. Lashbrook, U. S. Ozkan, J. Mol. Cat. A: Chem. 2004, 208, 233.

[20] S. Sugiyama, T. Miyamoto, H. Hayashi, M. Tanaka, J. B. Moffat, J. Mol. Cat. A: Chem. 1997, 118, 129.

[21] X. Sun, b. Li, H. Metiu, J. Phys. Chem. C 2013, 117, 23597.

[22] N. Mimura, I. Takahara, M. Inaba, M. Koamoto, K. Murata, Catal. Commun. 2002, 3, 257.

[23] X. Zhang, J. Liu, Y. Jing, Y. Xie, Appl. Catal. A: Gen. 2003, 240, 143.

[24] H. Zhu, D. C. Rosenfeld, D. H. Anjum, S. S. Sangaru, Y. Saih, S. Ould-Chikh, J. –M. Basset, J. Catal. 2015, 329, 291.

[25] T. T. Nguyen, M. Aouine, J. M. M. Millet, Catal. Commun. 2012, 21, 22.

[26] B. Fu, J. Lu, P. C. Stair, G. Xiao, M. C. Kung, H. H. Kung, J. Catal. 2013, 297, 289.

[27] P. Mars, D. W. van Krevelen, Chem. Eng. Sci. 1954, 3, 41.

[28] M. V. Martinez-Huerta, X. Gao, H. Tian, I. E. Wachs, J. L. G. Fierro, M. A. Banares, Catal. Today 2006, 118, 279.

[29] K. Grasselli, Top. Catal. 2002, 21, 79.

[30] O. R. Evans, A. T. Bell, T. D. Tilley, J. Catal. 2004, 226, 292.

[31] P. Concepción, A. Galli, J. M. L. Nieto, A. Dejoz, M. I. Vazquez, Top. Catal. 1996, 3, 451.

[32] J. L. Callahan, R. K. Grasselli, AIChE J. 1963, 9, 755.

[33] H. Zhu, D. C. Rosenfeld, M. Harb, D. H. Anjum, M. N. Hedhili, S. Ould-Chikh, J. –M. Basset, ACS Catal. 2016, 6, 2852.

[34] P. Botella, A. Dejoz, J. M. L. Nieto, P. Concepción, M. I. Vazquez, Appl. Catal. A: Gen. 2006, 298, 16.

[35] P. Botella, A. Dejoz, M. C. Abello, M. I. Vazquez, L. Arrua, J. M. L. Nieto, Catal. Today 2009, 142, 272.

[36] A. Trunschke in Nanostructured Catalysts-Selective Oxidations, Royal Society of Chemistry, Cambridge, 2011, pp. 5.

[37] B. Tope, Y. Zhu, J. A. Lercher, Catal. Today 2007, 123, 113.

[38] R. K. Grasselli, Top. Catal. 2001, 15, 93.

[39] Y. Wu, J. Gao, Y. He, T. Wu, Appl. Surf. Sci. 2012, 258, 4922.

[40] Z. Skoufa, G. Xantri, E. Heracleous, A. A. Lemonidou, Appl. Catal. A: Gen. 2014, 471, 107-117.

[41] H. Zhu, D. C. Rosenfeld, M. Harb, D. H. Anjum, M. N. Hedhili, S. Ould-Chikh, J.-M. Basset, ACS Catal. 2016, 6, 2852.

[42] B. Savova, S. Loridant, D. Filkova, J. M. M. Millet, Appl. Catal. A: Gen. 2010, 390, 148.

[43] B. Solsona, J. M. L. Nieto, P. Concepción, A. Dejoz, F. Ivars, M.I. Vázquez, J. Catal. 2011, 280, 28.

[44] Z. Skoufa, E. Heracleous, A. A. Lemonidou, J. Catal. 2015, 322, 118.

[45] E. Heracleous, A. A. Lemonidou, J. Catal. 2006, 237, 175.

[46] M. Alifanti, B. Baps, N. Blangenois, J. Naud, P. Grange, B. Delmon, Chem. Mater. 2013, 15, 395.

[47] R.D. Monte, J. Kašpar, J. Mater. Chem. 2005, 15, 633.

[48] H. -F. Lu, Y. Zhou, W. -F. Han, H. -F. Huang, Y. -F. Chen, Catal. Sci. Technol. 2013, 3, 1480.

[49] L. M. Toscani, A. F. Craievich, M. C. A. Fantini, D. G. Lamas, S. A. Larrondo, J. Phys. Chem. C 2016, 120, 24165.

[50] J. Santander, E. López, A. Diez, M. Dennehy, M. Pedernera, G. Tonetto, Chem. Eng. J. 2014, 255, 185.

[51] S. Letichevsky, C. A. Tellez, R. R. Avillez, M. I. P. Silva, M. A. Fraga, L. G. Appl. Catal. B: Environ. 2005, 58, 203.

[52] E. Heracleous, A. A. Lemonidou, J. Catal. 2010, 270, 67.

[53] E. Heracleous, A. A. Lemonidou, J. Catal. 2006, 237, 175.

[54] D. -W. Jeong, H. -S. Na, J. -O. Shim, W. -J. Jang, H. -S. Roh, Catal. Sci. Technol. 2015, 5, 3706.

[55] J. Li, X. Liu, W. Zhan, Y. Guo, Y. Guo, G. Lu, Catal. Sci. Technol. 2016, 6, 897.

[56] E. Heracleous, A. A. Lemonidou, J. Catal. 2006, 237, 162.

[57] Z. Skoufa, E. Heracleous, A. A. Lemonidou, Catal. Today 2012, 192, 169.

[58] B. Solsona, P. Concepción, S. Hernández, B. Demicol, J. M. L. Nieto, Catal. Today 2012, 180, 51.

[59] H. Zhu, D. C. Rosenfeld, D. H. Anjum, S. S. Sangaru, Y. Saih, S. Ould-Chikh, J. -M. Basset, J. Catal. 2015, 329, 291.

[60] T. Suzuki, A. Morikawa, A. Suda, H. Sobukawa, M. Sugiura, T. Kanazawa, J. Suzuki, T. Takada, R&D Review of Toyota CRDL 2002, 3737, 28.

[61] P. Manivasakan, P. Ramasamy, J. Kim, RSC Adv. 2015, 5, 33269.

[62] M. Jing, C. Wang, H. Hou, Z. Wu, Y. Zhu, Y. Yang, X. Jia, Y. Zhang, X. Ji, J. Power Sources 2015, 298, 241.

[63] Y. -Z. Su, Q. -Z. Xu, G. -F. Chen, H. Cheng, N. Li, Z. -Q. Liu, Electrochim. Acta 2015, 174, 1216.

[64] D. T. Dam, X. Wang, J. -M. Lee, ACS Appl. Mater. Interfaces 2014, 6, 8246.

[65] M. A. Peck, M. A. Langell, Chem. Mater. 2012, 24, 4483.

[66] B. Chu, H. An, T. A. Nijhuis, J. C. Schouten, Y. Cheng, J. Catal. 2015, 329, 471.

[67] E. W. McFarland, H. Metiu, Chem. Rev. 2013, 113, 4391.

[68] J. S. Valente, H. Armendáriz-Herrera, R. Quintana-Solórzano, P. d. Ángel, N. Nava, A. Massó, J. M. L. Nieto, ACS Catal. 2014, 4, 1292.

[69] G. Che-Galicia, R. Quintana-Solórzano, R. S. Ruiz-Martínez, J. S. Valente, C. O. Castillo-Araiza, Chem. Eng. J. 2014, 252, 75.

[70] J. S. Valente, R. Quintana-Solórzano, H. Armendáriz-Herrera, G. Barragán-Rodríguez, J. M. L. Nieto, Ind. Eng. Chem. Res. 2014, 53, 1775.

[71] F. Rahman, K. F. Loughlin, M. A. Al-Saleh, M. R. Saeed, N. M .Tukur, M. M. Hossain, K. Karim, A. Mamedov, Appl. Catal. A: Gen. 2010, 375, 17.

[72] F. Girgsdies, R. Schlögl, A. Trunschke, Catal. Commun. 2012, 18, 60.

[73] A. Celaya Sanfiz, T. W. Hansen, F. Girgsdies, O. Timpe, E. Rödel, T. Ressler, A. Trunschke, R. Schlögl, Top. Catal. 2008, 50, 19.

[74] T. T. Nguyen, M. Aouine, J. M. M. Millet, Catal. Commun. 2012, 21, 22.

[75] P. Botella, J. M. L. Nieto, B. Solsona, A. Mifsud, F. Marquez, J. Catal. 2002, 209, 445.

[76] M. Hävecker, S. Wrabetz, J. Kröhnert, L. -I. Csepei, R. N. d'Alnoncourt, Y. V. Kolen'ko, F. Girgsdies, R. Schlögl, A. Trunschke, J. catal. 2012, 285, 48.

국 문 초 록

최근들어, 경질 올레핀에 대한 수요 급증과 석유화학 원료에 대한 관심이 높아지면서 새로운 합성방법을 개발하는 연구가 지속되고 있다. 에틸렌은 폴리프로필렌, 산화에틸렌, 에틸렌글리콜, 스타이렌, 비닐아세테이트, PVC등 다양한 고분자 물질을 합성할 수 있는 원료로 사용되어 일상생활과 매우 밀접한 관계를 맺고 있는 물질이다.

현재까지 가장 널리 사용되어 오고 있으며, 상업화가 되어 있는 에틸렌 생산방법은 고온에서의 열분해를 통해 스팀을 활용한 크래킹방법이다. 이러한 스팀크래킹 방식에서 에틸렌을 생산하는데에 필요한 원료로는 나프타와 천연가스가 주로 사용되어 왔다. 하지만, 최근들어 북미 셰일가스 개발 및 동아시아의 천연가스 개발의 가속화로 인해 에탄의 가격이 안정화되고 수량확보가 용이해짐과 동시에 에탄을 원료로 사용하여 에틸렌을 생산하는 방식이 각광받고 있다. 특히, 기존의 스팀 크래킹 방식을 벗어나 더 경제적이고 친환경적인 방법으로 에틸렌을 생산할 수 있다고 알려져 있는 에탄의 산화탈수소반응 (oxidative dehydrogenation of ethane, ODHE)에 대한 관심이 증가하고 있는 추세이다.

이 공정은 앞서 설명한 다양한 장점을 가지고 있기 때문에 향후 지속가능한 연구주제로서 주목받고 있는 실정이다. 하지만, 높은 에탄 전환율과 에틸렌 선택도를 보일 수 있는 촉매의 개발이 미흡한 관계로 아직까지는 상업화 단계에 이르지 못하고 있다. ODHE반응을 통해 에틸렌을 생산할 수 있는 고효율 촉매 개발전략으로는 활성을 갖는 촉매의 외부적 혹은 내부적인 설계를 통한 물리화학적 특성을 향상시키는 것으로 아래와 나누어 생각해볼 수 있고, 해당 모델 전략을 아래와 같이 나타내었다.

- 외부적인 설계를 통한 촉매성능 향상을 위한 방법으로, 니켈-니오븀 혼합산화물에 세륨-지르코늄 혼합산화물을 도입하였다. 니켈-니오븀 산화물/세륨-지르코늄 혼합산화물을 사용하였을 때, 니켈-니오븀 혼합산화물만 존재할 때보다 이산화탄소, 일산화탄소, 메탄과 같은 부산물의 생성을 억제하는 현상을 관찰하였고, 반응온도의 증가를 통해 에탄 전환율의 상승에 기여할 수 있다는 것을 확인하였다. 결과적으로 에틸렌 수율을 증대시킬 수 있었다. 이러한 증진 요인을 알아보기 위해 전기화학 실험과 비교 반응성실험을 진행한 결과 세륨-지르코늄 산화물이 존재할 때, 니켈-니오븀 산화물 내의 니켈 이온이 화학양론적으로 잘 맞게 구성되어 있다는 것을 확인할 수 있었고, 이 두 가지 혼합산화물이 화학적인 상호작용을 할 수 있어야만 이러한 증

진 효과를 얻을 수 있다는 것을 확인할 수 있었다. 이러한 결과들을 통해 니켈-니오븀 혼합산화물의 산화/환원 특성이 증가하는 이유는 ODHE반응 도중 사용된 니켈-니오븀 산화물의 격자산소가 산소저장 및 공급에 유리하다고 알려진 세륨-지르코늄 산화물로부터 보충받을 수 있기 때문이라는 사실을 확인하였다.

- 내부적인 설계를 통한 촉매성능 향상을 위한 방법으로, 세륨이 도핑된 몰리브덴-바나듐-텔루리움-니오븀의 5금속 혼합산화물 촉매를 개발하였다. 이 연구에서는 5금속 혼합산화물 내에서 세륨의 역할을 정성적, 정량적으로 규명하고 그 영향이 ODHE 반응에서 어떻게 긍정적인 영향을 미칠 수 있는 지에 대한 내용들을 알아보고자 하였다. 첫 째로, 해당 5금속 혼합산화물이 에틸렌 생성에 유리한 상인 M1상을 가질 수 있는 합성 조건을 최적화 하는 실험을 진행하였고, 약 600 도씨에서 소성을 진행하였을 대 M1상의 비율이 가장 높다는 것을 확인하였다. 둘 째로, 도펀트로 사용된 세륨의 양을 최적화 시키는 과정을 거쳤으며, 약 0.1 몰 퍼센트의 세륨이 도핑되었을 때, 가장 높은 M1/M2 비율을 유지함을 확인하였다. 이 촉매는 ODHE반응 결과를 통해 세륨이 도핑되지 않았을 때와 동일한 수준의 에틸렌 수율을 보이는 기준에서 약 50 도씨의 반응온도를 낮출 수 있

다는 것을 확인하였다. 이 때의 에틸렌 선택도는 약 100%였다는 점을 미루어보아 동일 반응온도에서 에탄의 전환율이 상당히 증가할 수 있다는 것을 예상할 수 있다. 물리화학적 특성분석을 통해 세륨 이온이 5금속 혼합산화물에 도핑되어 있을 경우 활성점이 전자를 보유하고자 하는 성질이 강해진다는 것을 확인할 수 있었으며, 이는 즉, 주변의 반응물들을 산화시키는 데에 용이하다는 결과와 일치한다. 이를 통해 세륨 이온이 5금속 혼합산화물 격자 구조의 내부에서 화학결합을 통한 치환도핑이 되어 있다는 것을 확인할 수 있었으며, 향후 연구로는 세륨이온이 어떤 이온과 치환되어 있는지 알아보기 위한 연구가 진행되어야 할 것이다.

주요어: 불균일계 촉매, 산화탈수소반응, 에탄, 에틸렌, 격자산소

학 번: 2013-31305

List of publications

International Publications

International Peer-Reviewed Journals (First Author)

1. **M. Lee**[†], Y. S. Yun[†], J. Sung, J. Lee, Y.-J. Seo, I. K. Song, and J. Yi, "Enhanced ethylene productivity by the promotion of lattice oxygen in Ni-Nb-O/$Ce_xZr_{1-x}O_2$ composite for oxidative dehydrogenation of ethane", Catalysis Communications (2017) 95, 58-62. ([†]Equal contribution)
2. H. D. Song[†], **M. Lee**[†], G.-P. Kim†, I. Choi*, and J. Yi*, "Real time optical monitoring of Pt catalyst under the potentiodynamic conditions", Scientific Reports (Nature Publishing Group) (2016) 6, 38847. ([†]Equal contribution), (*Co-corresponding author)
3. G.-P. Kim[†], **M. Lee**[†], J. K. Jung, H. D. Song, and J. Yi, "Synthesis of highly dispersed porous Pt nanostructures via ionic diffusion control for enhanced electrocatalytic activity", Journal of Nanoscience and Nanotechnology, in press. ([†]Equal contribution)
4. G.-P. Kim[†], **M. Lee**[†], H. D. Song, S. Bae, and J. Yi, "Highly efficient supporting material derived from used cigarette filter for oxygen reduction reaction" Catalysis Communications (2016) 78, 1-6. ([†]Equal contribution)
5. **M. Lee**[†], G.-P. Kim[†], H. D. Song, S. Park, and J. Yi, "Preparation of energy storage material derived from used cigarette filter for supercapacitor electrode", Nanotechnology (2014) 25, 345601. ([†]Equal contribution)
6. **M. Lee**[†], H. J. Yun[†], S. Yu, and J. Yi, "Enhancement in photocatalytic oxygen evolution via water oxidation under visible light on nitrogen-doped TiO_2 nanorods with dominant reactive {102} facets", Catalysis Communications (2014) 43, 11-15. ([†]Equal contribution)
7. **D. M. Lee**[†], H. J. Yun†, S. Yu, S. J. Yun, S. Y. Lee, S. H. Kang, and J. Yi, "Design of an efficient photocatalytic reactor for the decomposition of gaseous organic

contaminants in air", Chemical Engineering Journal (2012) 187, 203-209. ([†]Equal contribution)

International Peer-Reviewed Journals (Co-author)

1. E. J. Lee, Y. J. Lee, J. K. Kim, **M. Lee**, J. Yi, J. R. Yoon, and I. K. Song, "Preparation and characterization of nitrogen-enriched carbon aerogel as a supercapacitor electrode materials", Journal of Nanoscience and Nanotechnology (2016) 16(10), 10413-10419.
2. G.-P. Kim, **M. Lee**, Y. J. Lee, S. Bae, H. D. Song, I. K. Song, and J. Yi, "Polymer-mediated synthesis of a nitrogen-doped carbon aerogel with highly dispersed Pt nanoparticles for enhanced electrocatalytic activity", Electrochimica Acta (2016) 193, 137-144.
3. Y. Kim, J. Y. Park, H. Y. Kim, **M. Lee**, J. Yi, and I. Choi, "Single nanoparticle-based sensor for hydrogen peroxide (H_2O_2) via cytochrome c-mediated plasmon resonance energy", Chemical Communications (2015) 51, 15370-15373.
4. E. J. Lee, Y. J. Lee, J. K. Kim, **M. Lee**, J. Yi, J. R. Yoon, J. C. Song, and I. K. Song, "Oxygen group-containing activated carbon aerogel as an electrode material for supercapacitor", Materials Research Bulletin (2015) 70, 209-214.
5. E.-G. Jung, Y. Shin, **M. Lee**, J. Yi, and T. Kang, "Interfacial synthesis of two-dimensional dendritic platinum nanoparticles using oleic acid-in-water emulsion", ACS Applied Materials & Interfaces (2015) 7(20), 10666-10670.
6. G.-P. Kim, S. Bae, **M. Lee**, H. D. Song, and J. Yi, "Decoration of a bio-inspired carbon nanosphere with Pt nanoparticles via a polymer-assisted strategy for enhanced electrocatalytic activity", Nano Energy (2015) 12, 675-685.
7. W. G. Moon, G.-P. Kim, **M. Lee**, H. D. Song, and J. Yi, "A bio-degradable gel electrolyte for use in high-performance flexible supercapacitors", ACS Applied Materials & Interfaces (2015) 7, 3503-3511.
8. H. J. Yun, **D. M. Lee**, S. Yu, J. Yoon, H.-J. Park, and J. Yi, "Effect of valence band energy on the photocatalytic performance of N-doped TiO_2 for the production

of O_2 via the oxidation of water by visible light", Journal of Molecular Catalysis A: Chemical (2013) 378, 221-226.

9. S. Yu, H. J. Yun, **D. M. Lee**, and J. Yi, "Preparation and characterization of Fe-doped TiO_2 nanoparticles as a support for a high performance CO oxidation catalyst", Journal of Materials Chemistry (2012) 22(25), 12629-12635.
10. H. J. Yun, H. Lee, N. D. Kim, **D. M. Lee**, S. Yu, and J. Yi, "A combination of two visible-light responsive photocatalysts for achieving the Z-scheme in the solid state", ACS Nano (2011) 5(5), 4084-4090.

Patents Application on File

1. 이종협, 김길표, **이민재**, 송현돈, 박수민, "비금속이 도핑된 수퍼 커패시터 전극용 다공성 탄소물질", 특허 등록 10-2015-0002563 (2015.01.08)
2. 이종협, 윤형진, **이민재**, 윤성진, "광촉매반응장치", 특허 출원 10-2010-0124241 (2010.12.07)

International Conferences (First author)

1. **M. Lee**, G.-P. Kim, H. D. Song, S. Bae, and J. Yi, "Used-cigarette filter induced electrocatalytic carbon support for efficient reduction of oxygen", 15th Korea-Japan Symposium on Catalysis, BEXCO and Haeundae Centum Hotel, Busan, Republic of Korea, (2015) 5/26 - 5/28.

International Conferences (Co-author)

1. Y. S. Yun, **M. Lee**, J. Sung, J. Lee, Y.-J. Seo, I. K. Song, J. Yi, "Enhanced redox property in Ni-Nb-O/$Ce_xZr_{1-x}O_2$ for selective production of ethylene from ethane", 16th Korea-Japan Symposium on Catalysis, Kaderu, Sapporo, Japan, (2017) 5/15 - 5/17.
2. H. Park, Y. S. Yun, D. Yun, T. Y. Kim, K. R. Lee, J. Baek, **M. Lee**, and J. Yi, "An

investigation of deactivation mechanism by coke via kinetics study of the glycerol dehydration over acid catalysts", 16th International Congress on Catalysis, China National Convention Center, Beijing, China, (2016) 7/3 - 7/8.

3. W. G. Moon, G.-P. Kim, **M. Lee**, and J. Yi, "Edible gel electrolyte derived from agarose for supercapacitor applications", 2014 The Korean Society of Clean Technology Fall Meeting, K hotel, Gyeongju, Republic of Korea, (2014) 9/24 - 9/26.
4. S. Park, I. Nam, G.-P. Kim, **M. Lee**, W. G. Moon, S. Bae, and J. Yi, "Robust hybrid film containing pseudocapacitive MnO_2 for large areal capacitance", 247th American Chemical Society National Meeting & Exposition, Dallas Convention Centre, Dallas, Texas, USA, (2014) 3/16 - 3/20.
5. H. J. Yun, H. Lee, **D. M. Lee**, S. Yu, and J. Yi, "Hydrogen Evolution via Water Splitting on Pt/CdS/Au/$TiO_{1.96}O_{0.04}$", 9th International Meeting of Pacific Rim Ceramic Societies, Cairns Convention Centre, Cairns, North Queensland, Australia, (2011) 7/10 - 7/14.
6. H. J. Yun, H. Lee, N. D. Kim, **M. Lee**, S. Yu, J. Baek, Y. Choi and J. Yi, "Facile adjustment of doping level in carbon doped TiO_2 nanoparticle", 218th The Electrochemical Society Meeting, Riviera Hotel, Las Vegas, Nevada, USA, (2010) 10/10 - 10/15.
7. H. J. Yun, H. Lee, N. D. Kim, **M. Lee**, S. Yu, and J. Yi, "Preparation and characterization of $TiO_{2-x}C_x$ nanoparticle for the high performance photo-catalyst, 18th International Conference on Photochemical Conversion and Storage of Solar Energy, Korea University, Seoul, Republic of Korea, (2010) 7/25 - 7/30.

Domestic Conferences

1. 이민재, 윤양식, 성종백, 송찬경, 이중원, 서영종, 송인규, 이종협, "Ni-Nb-O/$Ce_xZr_{1-x}O_2$의 향상된 산화환원능력을 통한 에탄 산화탈수소반응용 촉매 제조 및 에틸렌 생산능력 평가", 한국청정기술학회 춘계 학술발표회, 부산 웨스틴조선호텔, (2017) 3/29 - 3/31.

2. **이민재**, 김길표, 이윤재, 배성준, 송현돈, 송인규, 윤양식, 김윤화, 이종협, “탄소 에어로겔의 고분자 기능화를 통한 고분산 백금 나노촉매 개발 및 전기화학적 성능평가”, 한국화학공학회 춘계 총회 및 학술대회, 부산 BEXCO, (2016) 4/27 - 4/29 (Oral).
3. **이민재**, 김길표, 송현돈, 이종협, “환경친화형 휘어지는 슈퍼커패시터 개발”, 한국화학공학회 춘계 총회 및 학술대회, 제주국제컨벤션센터, (2015) 4/22 - 4/24 (Oral).
4. **이민재**, 김길표, 송현돈, 이종협, “고분자 매개체를 활용한 고분산 백금 나노촉매의 개발 및 성능평가”, 한국전기화학회 춘계 총회 및 학술발표회, 광주김대중컨벤션센터, (2015) 4/2 - 4/4.
5. **이민재**, 김길표, 송현돈, 이종협, “무독성 한천 겔 전해질을 이용한 휠 수 있는 수퍼커패시터 개발 및 전기화학적 성능 평가”, 한국청정기술학회 춘계 학술발표회, 부여 롯데리조트, (2015) 3/26 - 3/27.
6. **이민재**, 김길표, 송현돈, 이종협, “3차원 탄소표면의 고분자 기능화를 통한 고분산 백금 나노촉매 제조 및 전기화학적 성능평가”, 한국청정기술학회 춘계 학술발표회, 부여 롯데리조트, (2015) 3/26 - 3/27.
7. **이민재**, 김길표, 송현돈, 박수민, 문원균, 이종협, “사용된 담배필터를 재활용한 기공성 탄소제조 및 수퍼커패시터 성능평가”, 한국청정기술학회 춘계 학술발표회, 여수경도리조트, (2014) 3/27 - 3/28.
8. **이민재**, 윤형진, 유성주, 여정은, 이종협, “질소도핑 TiO_2 가시광 광촉매의 도핑수준이 물산화 반응의 성능에 미치는 영향”, 한국화학공학회 추계 총회 및 학술대회, 송도컨벤시아, (2011) 10/26 - 10/28.
9. **이민재**, 윤형진, 이현주, 김남동, 유성주, 이종협, “Hydrogen evolution via water-splitting by artificial Z-scheme photocatalyst under the irradiation of visible light”, 18th Annual Meeting for Korean Society of Photoscience, 서강대학교, (2011) 6/9 - 6/10.
10. **이민재**, 윤형진, 이선용, 유성주, 강상현, 윤성진, 이종협, “UV/TiO_2 광촉매 시스템을 이용한 DMS 기상분해반응”, 한국화학공학회 추계 총회 및 학술대회, 대전컨벤션센터, (2010) 10/20 - 10/22.
11. 김유라, 박지윤, **이민재**, 이종협, 최인희, “Single nanoparticle based sensor of

reactive oxygen species (ROS) via cytochrome c mediated plasmon resonance energy transfer", 한국화학공학회 춘계 총회 및 학술대회, 제주국제컨벤션센터, (2015) 4/22 - 4/24.

12. 박홍석, 윤양식, 김길표, **이민재**, 송현돈, 서영종, 김왕규, 이중원, 이종협, "산 촉매에서의 글리세롤 탈수반응에 대한 반응속도론적 연구", 한국화학공학회 추계 총회 및 학술대회, 대전컨벤션센터, (2014) 10/23 - 10/24.
13. 남인호, 김길표, 박수민, 송현돈, **이민재**, 문원균, 배성준, 이종협, "대면적의 패턴화된 망간 산화물 수퍼커패시터 개발 및 성능 평가", 한국전기화학회 추계 총회 및 학술발표회, 대전컨벤션센터, (2013) 11/7 - 11/9.
14. 박수민, 남인호, 김길표, 문원균, 배성준, **이민재**, 송현돈, 이종협, "박막전지의 구조적 안정성을 높이기 위한 유기겔-금속산화물 복합체 합성", 한국전기화학회 추계 총회 및 학술발표회, 대전컨벤션센터, (2013) 11/7 - 11/9.
15. 김길표, 박수민, 남인호, 송현돈, **이민재**, 배성준, 문원균, 이종협, "전기화학 증착법을 이용한 이방성 결정구조를 지닌 연결된 기공구조의 NiO 합성 및 리튬이온 배터리 음극 활용", 한국전기화학회 추계 총회 및 학술발표회, 대전컨벤션센터, (2013) 11/7 - 11/9.
16. 유성주, **이민재**, 김혜선, 이수영, 김용화, 이종협, "물 산화반응에 적합한 표면구조의 질소도핑 TiO_2 나노입자 개발", 한국청정기술학회 추계 학술발표회, 제주 한화리조트, (2013) 9/25 - 9/27.
17. 유성주, 윤형진, **이민재**, 이종협, "철 도핑 TiO_2를 이용한 금 나노촉매의 일산화탄소 산화반응", 한국화학공학회 추계 총회 및 학술대회, 송도컨벤시아, (2011) 10/26 - 10/28.
18. 유성주, 윤형진, **이민재**, 이종협, "고분자전해질 연료전지의 피독현상 방지를 위한 고성능 일산화탄소 산화촉매 개발", 한국에너지공학회 추계 총회 및 학술대회, 서울대학교 교수회관, (2011) 10/20 - 10/21.
19. 윤형진, 김남동, **이민재**, 유성주, 여정은, 이종협, "고체 상에서의 Z-Scheme 구현을 통한 물분해 수소생산", 한국에너지공학회 추계 총회 및

학술대회, 서울대학교 교수회관, (2011) 10/20 - 10/21.

20. 유성주, 윤형진, **이민재**, 이종협, “일산화탄소의 산화반응을 위한 Au/Fe-TiO_2 촉매의 제조 및 분석, “한국화학공학회 춘계 총회 및 학술대회, 창원컨벤션센터, (2011) 4/27 - 4/29.
21. 윤형진, 이현주, 김남동, **이민재**, 유성주, 이종협, “나노물질기반의 물분해 수소생산을 위한 인공광합성 구현”, 한국화학공학회 춘계 총회 및 학술대회, 창원컨벤션센터, (2011) 4/27 - 4/29.
22. 윤형진, **이민재**, 유성주, 백자연, 최영보, 이종협, “다양한 형태의 TiO_2 나노입자 제조 및 광촉매 특성 변화”, 한국청정기술학회 추계 학술발표회, 충남대학교, (2010) 11/19.
23. 윤형진, 이현주, 김남동, **이민재**, 이종협, “$TiO_{2-x}C_x$ 광촉매 나노입자의 합성 및 밴드갭 에너지 조절”, 한국화학공학회 춘계 총회 및 학술대회, 대구 EXCO, (2010) 4/21 - 4/23.